

Radio Interferometric Planet Search I: First Constraints on Planetary Companions for Nearby, Low-Mass Stars from Radio Astrometry

Geoffrey C. Bower¹, Alberto Bolatto^{1,2}, Eric B. Ford^{1,3}, Paul Kalas¹

gbower@astro.berkeley.edu

ABSTRACT

Radio astrometry of nearby, low-mass stars has the potential to be a powerful tool for the discovery and characterization of planetary companions. We present a Very Large Array survey of 172 active M dwarfs at distances of less than 10 pc. Twenty nine stars were detected with flux densities greater than $100 \mu\text{Jy}$. We observed 7 of these stars with the Very Long Baseline Array at milliarcsecond resolution in three separate epochs. With a detection threshold of $500 \mu\text{Jy}$ in images of sensitivity $1\sigma \sim 100 \mu\text{Jy}$, we detected three stars three times (GJ 65B, GJ896A, GJ 4247), one star twice (GJ 285), and one star once (GJ 803). Two stars were undetected (GJ 412B and GJ 1224). For the four stars detected in multiple epochs, residuals from the optically-determined apparent motions have an rms deviation of ~ 0.2 milliarcseconds, consistent with statistical noise limits. Combined with previous optical astrometry, these residuals provide acceleration upper limits that allow us to exclude planetary companions more massive than $3 - 6 M_{Jup}$ at a distance of ~ 1 AU with a 99% confidence level.

Subject headings: astrometry,stars:activity,stars:early-type,stars:planetary systems,radio continuum: stars

1. Introduction

The study of extrasolar planets provides an important link between the study of star formation, the study of our own solar system, and the search for extraterrestrial life. During the past two decades, radial velocity surveys have over 300 extrasolar planets with

¹Astronomy Department & Radio Astronomy Laboratory, University of California, Berkeley, CA 94720

²Department of Astronomy, University of Maryland, College Park, MD, 20742-2421

³Astronomy Department, University of Florida, Gainesville, FL 32611-2055

$m_p \sin i \leq 13M_J$ (Butler et al. 2006b, www.exoplanets.org; www.exoplanet.eu). Doppler surveys show that $\sim 10.5\%$ of nearby solary-type (FGK) stars have planets with orbital periods less than 2000 days (Cumming et al. 2008).

Unfortunately, several factors make it difficult for radial velocity searches to detect planets around M dwarfs (e.g., paucity of narrow spectral lines, reduced flux, photospheric and chromospheric activity; see Joergens (2006)). From the eight M star planetary systems detected by radial velocity techniques (Bailey et al. 2009), GJ 876 is particularly interesting because it has a short-period $\sim 7.5 M_\oplus$ planet (Rivera et al. 2005), as well as a pair of massive planets with orbital periods of ~ 30 and ~ 60 days in a 2:1 mean motion resonance (Laughlin et al. 2005). Benedict et al. (2002) measured an astrometric perturbation by GJ 876d of $0.25 \pm 0.06\text{mas}$. GJ 849 is noteworthy because it hosts a giant planet ($\sim 0.8M_J$) with an orbital period of ~ 5.1 years (Butler et al. 2006a). Johnson et al. (2007) found evidence for at least one and perhaps two giant planets orbiting GJ 317 at separations of ~ 1 AU or more. Planets around GJ 849b and GJ 317b are estimated to induce astrometric perturbations of $\sim 0.6\text{mas}$ and $\sim 0.5\text{mas}$ (Butler et al. 2006a; Johnson et al. 2007). Most recently, GJ 832 was found to have a Jupiter mass planet in a nine-year orbit (Bailey et al. 2009), whereas GJ 176 has a super-Earth on a nine-day orbit (Forveille et al. 2009). Overall, the Jupiter-mass M dwarf planets have astrometric signals that are comparable to those detectable with radio astrometric techniques.

The radial velocity results allow estimates of the frequency of short-period giant planets around M dwarfs. Endl et al. (2006) estimate a frequency of close-in Jovian planets around M dwarfs of $\leq 1.3\%$. Johnson et al. (2007) estimate the low-mass K and dM stars have a $1.8 \pm 1.0\%$ planet occurrence rate, significantly less than that for solar-mass stars ($4.2 \pm 0.7\%$). Several groups are working to extend the Doppler technique to the near-infrared (e.g., Lloyd et al. 2009; Ramsey et al. 2008; Ge et al. 2006), though initial results will still be biased towards short orbital periods. Thus, it is interesting to consider alternative techniques which are best suited for searching M dwarfs for planets at larger separations.

The microlensing technique has discovered several extrasolar planets around low-mass stars. For example, (Gaudi et al. 2008) present evidence for two giant planets with orbital separations of ~ 2.3 and $\sim 4.6\text{AU}$. This and two other systems (Udalski et al. 2005; Dong et al. 2008) provide evidence for roughly Jupiter mass planets. The host stars of the systems discovered by microlensing are too distant to lead to a detectable astrometric signature. However, they do provide further evidence for a population of planets with separations and orbital periods that are well-suited for astrometric detection when considering nearby M dwarfs. Other detections (Bennett et al. 2008; Beaulieu et al. 2006; Gould et al. 2006) suggest that lower-mass planets may be quite common around M dwarfs.

Direct imaging has been used to detect planet candidates in wide orbits around several low-mass stars (Chauvin et al. 2004, 2005; Neuhäuser et al. 2005). While these planets would induce a large astrometric perturbation, their long orbital periods would make it impractical to discover such planets from astrometry alone. The low density of bright M dwarfs on the sky makes transit searches particularly difficult. However, the potential for detecting transiting planets near the habitable zone of an M dwarf has motivated at least one dedicated M dwarf transit search (Irwin et al. 2009). Due to the strong bias towards finding short-period planets, the transit technique (like the Doppler technique) is complementary to microlensing, direct imaging, and astrometric searches that are best suited for planets with wider orbits.

Optical astrometry has been used to search for planets around nearby M dwarfs (Pravdo & Shaklan 1996, 2003), leading to discovery of several low mass companions (Pravdo et al. 2005). These studies are fore-runners of space-based astrometric planet searches such as with SIM Shao & Nemati (2009).

In this paper, we focus on the potential for a ground-based astrometric planet search using techniques of radio astronomy. Radio astrometry has long been the gold standard for definition of celestial reference frames (Fey et al. 2004) and has been used to obtain the most accurate geometric measurements of any astronomical technique. Astrometric results include measurement of the parallax and proper motion of pulsars at distances greater than 1 kpc (Brisken et al. 2002), an upper limit to the proper motion of Sagittarius A* of a few km s^{-1} (Reid & Brunthaler 2004), a $< 1\%$ distance to the Taurus star-forming cluster (Loinard et al. 2007) and to Ophiuchus (Loinard et al. 2008), a $\sim 5\%$ distance to the Orion Nebula star-forming cluster (Sandstrom et al. 2007; Menten et al. 2007), and accurate parallaxes to star-forming regions at distances as large as 5 kpc (e.g., Xu et al. 2009).

Many radio-astrometric studies have been performed on stars. Very long baseline interferometry (VLBI) has been used to astrometrically discover the low-mass ($M \approx 0.1 M_{\odot}$) companion of the southern hemisphere K dwarf AB Doradus and characterize its orbit (Gould et al. 2006) Similarly, VLBI studies of radio-emitting stars have been used to link the reference frame of the HIPPARCOS satellite to the radio extragalactic reference frame and study the orbit of the ternary system Algol (Lestrade et al. 1999), and study the structure of the radio emission in T Tauri stars (Phillips et al. 1996). In fact, T Tauri itself has been the target of a number of astrometric studies in the radio (e.g., Loinard et al. 2007). The Very Long Baseline Array (VLBA) can routinely achieve an astrometric accuracy of $\sim 100 \mu\text{as}$ in a single epoch, and it is capable of accuracies as high as $8 \mu\text{as}$ under favorable circumstances (Fomalont & Kopeikin 2003). To use this technique the target source must have a sufficiently high brightness temperature to be detected by a high resolution radio interferometer. For the VLBA, brightness temperatures must be $T_b > 10^7$ K, requiring nonthermal emission.

Thus, the systems which can be studied are limited to the most active stars.

Nonthermal stellar radio emission has been detected from many stellar types (Güdel 2002), including brown dwarfs (Berger 2006), proto-stars (Bower et al. 2003), and massive stars with winds (Dougherty et al. 2005). Radio emission from the late-type stars was first detected by Gary & Linsky (1981) and it originates in cyclotron emission due to non-relativistic electrons in the coronal plasma. Only late-type stars are sufficiently bright, numerous, and low mass to provide a large sample of stars suitable for large-scale astrometric exoplanet searches. Radio astrometric searches can determine whether or not M dwarfs, the largest stellar constituent of the Galaxy, are surrounded by planetary systems as frequently as FGK stars and how the planet mass-period-eccentricity relation varies with stellar type. While Doppler and transit methods can constrain this distribution at short-orbital periods, astrometry is best suited for studying planets at a few AU, where they induce a large astrometric signal and it is still practical to observe the system for multiple orbital periods. The population of gas giants at a few AU around low mass stars is an important discriminant between planet formation models (e.g., Laughlin et al. 2004; Ida & Lin 2005; Boss 2006; Kennedy et al. 2007).

Radio astrometric searches for planets have a number of unique qualities. First and foremost, searches in the radio observe stars that because of their activity and variability are not good targets for radial velocity or transit studies. Thus they are highly complementary to those carried out using other techniques. Furthermore, astrometric studies of reflex motion have the ability to fully characterize the orbits and masses of the detected planets, without the degeneracies inherent to radial velocity techniques. Finally, they are sensitive to long-period planets with sub-Jovian masses provided there is a long-enough time baseline of observations, and they naturally provide absolute astrometric positions tied to the extragalactic reference frame.

The most serious limitation to astrometric accuracy may be from stellar activity that results in an astrophysical “jitter” added to the true source position. Most evidence, however, indicates that this jitter is small enough to permit exoplanet searches around nearby stars. For instance, White et al. (1994) model the radio emission of dMe stars as originating within ~ 1 stellar radius of the photosphere. At a distance of 10 pc for a M5 dwarf, a stellar radius is ~ 0.1 mas, an order of magnitude smaller than the astrometric signature of a Jupiter analog. The few dwarf stars detected with VLBI appear to be compact, supporting this result (Benz et al. 1998; Guirado et al. 2006).

High quality astrometric positions of radio stars are also critical for connecting radio and optical reference frames (Perryman et al. 1997; Lestrade et al. 1999; Boboltz et al. 2007). Additionally, these observations will produce sizes, morphologies and brightness tempera-

tures critical for the study of physical processes in active stars, which are poorly understood (e.g., Güdel 2002; Berger 2006).

In this paper, we provide results from a flux density survey of nearby, low mass stars (§2 and 3). In §4, we present multi-epoch, high-resolution astrometric observations of a subset of the detected stars. In §5, we calculate limits on companions based on the radio measurements and archival optical astrometry. We summarize in §6.

The observations described in this paper constitute a preliminary survey for the Radio Interferometric Planet (RIPL) search. RIPL is a program with the VLBA and the 100-m Green Bank Telescope with the goal of astrometric detection of companions to nearby, low mass stars (Bower et al. 2007). A sample of 30 stars taken from the VLA surveys described below will be observed 12 times over ~ 3 years with an astrometric accuracy of ~ 0.1 mas, sufficient to detect Jupiter mass companions at a radius of 1 AU. The results of this paper demonstrate that jitter in stellar position is not a limiting factor for RIPL.

2. Sample Definition

Stars were drawn from two samples: active stars in the California & Carnegie planet search (Wright 2005) and X-ray selected nearby stars which are too active for radial velocity searches (NEXXUS Schmitt & Liefke 2004). X-ray fluxes are from the ROSAT all sky survey. The most active of the California & Carnegie stars had a lower X-ray luminosity than the least active of the NEXXUS stars. All stars are M dwarfs at $D < 10$ pc. In addition, we include three stars, GJ436 (M2.5 Butler et al. 2004), ϵ Eri (K2V Campbell et al. 1988; Cumming et al. 1999) and HD 131156 (G8V), which are chromospherically active, nearby, and show radial velocity signatures for planetary companions (ϵ Eri has also a nearly face-on debris disk; Greaves et al. (1998)). We also include the dMe star AU Mic (GJ 803) which has a recently discovered nearly edge-on debris disk (Kalas et al. 2004), since debris disks are believed to be signposts of planet formation. Basic stellar data for 172 stars are tabulated in Table 1. These data comprise extended Gliese catalog number, coordinates, error ellipse in position, proper motion, error ellipse in proper motion, annual parallax and its error, spectral type, apparent B and V magnitudes and X-ray luminosity.

3. Flux Density Observations

We used the Very Large Array to observe our sample in June through September 2005. Observations were made at 5 GHz in standard continuum mode. The array was in B, C, and

D configurations, giving a resolution that ranged from ~ 1 to 10 arcsec. Each source was observed for 10 minutes per epoch; some sources were observed multiple times. Standard calibration and imaging techniques were applied with AIPS (Greisen 2003). The typical image rms was $\sim 50\mu\text{Jy}$.

In Table 2 we list flux densities for sources detected in at least one epoch. We made 40 detections of 29 individual stars. In Table 3, we list upper limits to the flux density for sources that were not detected.

We plot the radio and X-ray luminosities for the detected and non-detected stars in Figure 1. X-ray luminosities are from the ROSAT survey and so are non-contemporaneous with radio observations. Nevertheless, we see rough agreement with the radio-X-ray luminosity correlation (Güdel 2002). We also separate late and early type stars at type M5 but find no difference in detection rates or flux densities.

4. VLBA Astrometric Survey

4.1. Observations and Data Analysis

In Spring, 2006, we studied the astrometric stability of seven stars with the VLBA. These stars were selected as among the brightest stars from the VLA sample. For each star, three VLBA epochs were spread over 11 days or less (Table 4). Observations were obtained at a frequency of 8.4 GHz with a recording bandwidth of 256 Mb/sec. Phase-referenced observations were obtained for each of the stars with an integration time on the star of ~ 1 hour distributed over 4 to 8 hours, achieving an rms sensitivity of $\sim 100\mu\text{Jy}$. Beam sizes and rms flux densities for each epoch are in Table 4.

Data were processed using the VLBA pipeline in AIPS. Standard amplitude and phase calibration techniques were employed. The positions and flux densities of primary and secondary calibrators are listed in Table 5. In the case of primary calibrators, the positions are those assumed for correlation. These positions were taken from VLBA calibrator lists and are typically accurate in an absolute sense to a milli-arcsecond. Secondary calibrator positions were determined by phase referencing to the primary calibrator. The reported positions and flux densities are the averages over the three epochs.

4.2. Astrometry

Of the 7 stars observed by the VLBA, three stars (GJ 4247, GJ 65B, and GJ 896A) were detected in all three epochs, one star (GJ 285) was detected in two epochs, one star was detected in only one epoch (GJ 803), and two stars were not detected in any epoch (GJ 1224). The detections had flux densities ranging from 0.5 to 3.9 m Jy (equivalent to $\text{SNR} \sim 5$ to 20). Images were reasonably well-fit as point sources; we discuss possible deviations from point source images later. Best-fit positions and flux densities are given in Table 6. We show images of the stars and their primary and secondary calibrators in Figures 2, 3, 4, 5, 6, 7, 8,

In the second epoch of observation, GJ 285 was not detected and we show an image at its expected position. The secondary calibrators were imaged indicating that phase-referencing was successful. The absence of GJ 285 thus must be attributed to a flux density below the 3σ -limit of $\sim 300 \mu\text{Jy}$ or to resolved structure.

GJ 65B has a large apparent motion ($\sim 16 \text{ mas/day}$) and was significantly variable during the experiment. The apparent motion due to both its large proper motion and large parallax causes the source to move more than a beam width during the 5 hours of observation. We split epochs into two time ranges and found significant variability in the flux density. In the first epoch, GJ 65B is detected in both halves of the epoch. In the second and third epochs, GJ 65B is detected in only the second half of each epoch. Observational results are tabulated for these four half epochs in which GJ 65B is detected.

We detected GJ 803 in only epoch. In the second epoch, phase stability was very poor such that the images of the calibrators were severely distorted. In the third epoch, the calibrator images were of good quality but there was no detection of GJ 803 at a level of 5σ within the field of view anticipated given the detection in the first epoch and optical astrometry. Imaging quality is poor for this source due to its low declination. For second and third epochs, we show images at the expected locations of the star, assuming optical proper motions and parallaxes and the position detected in the first epoch.

Detections were not obtained in any epoch for two stars, GJ 412B and GJ 1224. Observing conditions for GJ 412B were good on all three epochs but no source was detected. Compact calibrators J1110+44 and J1058+43 were detected with consistent flux density, structure, and positions in all three epochs. GJ 412B is separated from the calibrator by approximately $30'$, which is less than the separation of the secondary calibrators. Thus, poor phase calibration is unlikely to be the cause for the lack of detection of GJ 412B. Based on optical astrometry, the apparent position of GJ 412B was changing during these epochs at a rate $\sim 0.6 \text{ mas h}^{-1}$, which means that it moved more than a synthesized beam width during

the course of the observations. If uncorrected, this leads to an approximately 40% reduction in the observed peak flux density. We corrected for this effect by making images from short time segments, shifting the positions of these segments to account for the optical astrometric model, and then co-adding these segments. The star was not detected in the final co-added images. We searched images that were $\sim 2.2''$ on a side, centered on the optical position. The likely cause of the lack of detection is low flux density. In two out of three VLA epochs, GJ 412B was not detected above $200 \mu\text{Jy}$.

In the case of GJ 1224, phase-referencing failed. This is due to the large offset in declination (~ 3 degrees) between the phase calibrator J1753-1843 and the star. The image of secondary calibrator J1809-152, which is within 0.7 deg of GJ 1224, showed the effects of poor phase calibration. On the other hand, the secondary calibrator J1825-1718 is within a degree in declination of the primary calibrator and was observed to have a relatively compact structure. Self-calibrated observation of J1809-152 indicate a compact source with 60 mJy flux density, suitable as a phase calibrator for future observations of GJ 1224.

5. Discussion

5.1. Survey Images

The VLBA images in our exploratory survey, with the exception of that for GJ65B, are predominantly compact and point-like. This is consistent with the radio emission originating from points close to the stellar photosphere, which has a characteristic radius of $R_* \approx 0.1R_\odot$ (equivalent to $\theta_* \approx 100 \mu\text{as}$ at a distance of 5 pc ; Beatty et al. 2007).

The image of GJ65B (also known as UV CET B) is extended, as was previously seen by Benz et al. (1998). The image appears to consist of two components, possibly with a variable position angle. Benz et al. (1998) argue that these two components are magnetic loops in the corona and that the star is located between these two. We find that the flux density of GJ65B is variable, as was previously observed (Linsky & Gary 1983; Pallavicini et al. 1985; Jackson et al. 1987).

GJ 896A (EQ Peg) has been previously detected with VLBI and found to be compact (Benz et al. 1995). GJ 285 (YZ CMi) has been previously detected as compact and marginally resolved with VLBI in different epochs (Benz & Alef 1991; Pestalozzi et al. 2000). GJ 803 and 4247 have not been previously imaged with VLBI to our knowledge. We leave a detailed investigation of stellar activity to another paper.

5.2. Astrometric Results

For the four sources (GJ 896A, GJ 4247, GJ 65B, and GJ 285) detected in multiple epochs, we plot their positions as a function of time in Figures 9 through 12. Positions are referred to the expected position for the first epoch from the existing optically-determined astrometry, proper motion, and parallax listed in Table 1. These originate from Hipparcos observations for GJ 285 and GJ 896A (Perryman et al. 1997), from a comparison of the Luyten and 2MASS catalogs for GJ 65B (Salim & Gould 2003), and from a comparison of the Luyten and Tycho-2 catalogs for GJ 4247 (Lépine & Shara 2005). In Table 6, we tabulate the radio coordinates relative to the first epoch VLBA position ($\Delta\alpha$, $\Delta\delta$) and to the expected optical positions ($\Delta\alpha_{\text{opt}}$, $\Delta\delta_{\text{opt}}$).

We have compared the measured positions of the radio stars with their predicted optical positions. The uncertainties in the radio-optical position offsets are dominated by the relatively large astrometric uncertainties in the optical measurements, primarily due to the faintness of the stars and the long time baseline between the optical and VLBA measurements. As an ensemble, the mean positions are consistent with no offset. The reduced χ^2 is 0.8 and 0.7 for α and δ , respectively. The positions measured by the VLBA are consistent with the optical astrometry for GJ 4247, GJ 803, and GJ 285 in both coordinates. In the case of GJ896A, there is a marginal detection (3.2σ) of an offset in the absolute right ascension. In the case of GJ65B, the total radio-optical offset is also marginally significant. As we discuss below, this source is part of a binary, which complicates the interpretation of these short observations.

The RMS residuals relative to the optical astrometry in each coordinate are ~ 0.1 to ~ 0.2 mas (Figures 9, 10, 11, and 12). This RMS is consistent with statistical errors in the VLBA observations, indicating that there is not a significant contribution to the source positions from stellar activity. The absence of a stellar activity contribution to the astrometry is a central result of this paper. It remains possible that the emission originates from a region that is a few stellar radii in scale but has a stable centroid on a time-scale of days. It is also possible that there is longer-term stellar activity that will corrupt astrometric accuracy.

We have also compared the relative apparent motions of our sources. For all sources, we compute the difference in the apparent motions determined by VLBA and that from the optical catalogs ($\Delta\mu_\alpha$ and $\Delta\mu_\delta$; Table 7). These apparent motions include the effects of parallax and proper motion. We then compute the implied acceleration in each coordinate using the time difference between the epoch of the VLBA observations and the epoch of the optical position determinations. For Hipparcos observations, the epoch of the optical observations is 1991.25. For the other two catalogs, we take the epoch of proper motion as the mean of the Luyten catalog epoch (1950) and the relevant modern optical catalog, either

2MASS (epoch 1999) or Tycho-2 (epoch 1991.25). The uncertainty in acceleration has a significant component set by the relatively short time-baseline of the VLBA measurements. For the cases of GJ 65B and GJ 4247, the VLBA observations span only 3 days, which leads to an error in apparent motion of $\sim 0.2 \text{ mas}/3 \text{ days} \sim 25 \text{ mas/year}$. Observations that span a year will be one to two orders of magnitude more sensitive to acceleration.

For all stars but GJ 65B, there is no detection of an apparent acceleration relative to the optical astrometry. In the case of GJ 65B there is a significant offset (6σ) in the declination proper motion. The right ascension proper motion is fully consistent with statistical errors in the VLBA measurements. As we discuss below, the apparent acceleration for GJ 65B is consistent with the expectations for the binary orbit.

5.3. Limits on Companion Mass and Semi-Major Axis

For the stars for which we find an upper limit on the acceleration, we compute limits on companion mass and semi-major axis, assuming circular orbits. We assume a mass of $0.1 M_{\odot}$ for the star. Our calculation determines the fraction of systems with which a 3σ detection is made for a given set of planetary mass and semi-major axis.

The reflex motion, R , of a star of mass M due to an orbiting planet of mass M_p orbiting a distance r away from the center of mass of the system can be simply expressed as

$$R = -\frac{M_p}{M}r. \quad (1)$$

Assuming a circular orbit, the instantaneous star speed and acceleration are

$$\frac{dR}{dt} \propto \frac{M_p}{\sqrt{Mr}} \quad (2)$$

$$\frac{d^2R}{dt^2} \propto \frac{M_p}{r^2} \quad (3)$$

where r is the orbital semimajor axis of the planet and we assume $m \ll M$. At small semi-major axes, limits on companion mass and semi-major axis are set by the maximum angular displacement of the star during the period covered by the observations. At these small separations, accelerations larger than the minimum observable acceleration can occur, but these do not produce an angular displacement detectable by the VLBA. We have calculated the acceleration of the star, projecting the systems over the full range of stellar positions and

orbital inclination angles and sum over all systems that produce a detectable offset. This effect then incorporates the loss due to systems with an orbital period much less than the baseline time. The corresponding limit on companion masses then scales as r^{-1} .

At large star-planet separations (r) — and therefore long periods — the limits are set by the acceleration due to the companion. The fraction of systems that have detectable accelerations for a given radius are a function of the inclination angle of the binary and the position angle of the two proper motion measurements. To determine our confidence limits we compute the acceleration for a face-on system and then project the orbit onto a full range of position and inclination angles and sum over all systems that produce an acceleration greater than our acceleration limits. The calculation does not take into account the degenerate condition that occurs when the period is very close to the separation between the optical and radio epochs. For stars with Hipparcos data, this peak is at 15 years, corresponding to 3 AU for the $0.1 M_{\odot}$ star; for the other stars, the time baseline is > 30 to 50 years. The mass limits scales with distance to the star as r^2 (see Eq. 3). Acceleration limits are three times the quadrature sum of the errors in the two coordinates.

For the data presented here the acceleration limits correspond to a minimum in mass at an approximate semi-major orbital axis $r_{min} \sim 1$ AU (Figures 13). That is, these observations are most sensitive to planets orbiting at that distance from the primary. Near this minimum the orbital periods are ~ 3 years and the minima in mass ($M_{p,min}$) are in the range 2 to 5 M_{Jup} (Table 8). We also give the planet mass detection thresholds at 0.3 AU ($M_{p,0.3}$) and 3 AU ($M_{p,3}$); these are in the range of 10 to 20 M_J and 20 to 40 M_J , respectively.

To be conservative, we treat the detection of acceleration for GJ65B as an upper limit as well. For the nominal acceleration detection, $a = 0.0192 \pm 0.0038 \text{ AU/yr}^2$, solutions for $r > 1.4$ AU fall on the curve

$$\left(\frac{M_p}{4.5 M_{Jup}} \right) = \left(\frac{r}{3 \text{ AU}} \right)^2. \quad (4)$$

GJ65B has an M dwarf companion with an orbital period $P = 26.52$ yr, inclination $i = 127^\circ$, and semimajor axis $a = 1.95$ arcsec or 6.3 AU (Geyer et al. 1988). The maximum apparent acceleration for this system is 0.083 AU/yr^2 . Observations at non-optimal epochs (as we have in this case) will lead to reduced apparent acceleration, consistent with the acceleration we have observed.

It is difficult to model exactly the contribution of the binary orbit to the proper motion and acceleration of GJ65B given uncertainty over exact observing epochs and methods for calculating the published proper motions based on optical observations. But it appears that the

binary orbit was not taken into account in the proper motion calculation of Salim & Gould (2003). For epoch 1950 of the Luyten catalog and epoch 2006 of the VLBA observations, the star was near apastron while for epoch 1999 of the 2MASS catalog the star was near periastron. We estimate an additional error of (10, 30) mas/y in the right ascension and declination proper motions based on the stellar orbit. This has the effect of reducing the significance of $\Delta\mu_\delta$ and the acceleration a_δ to less than 5σ . We also note that observations at low declination are prone to more systematic error in the declination coordinate.

GJ896A is also in a close binary system with another low mass star. We are unaware of an orbital solution for the system and therefore cannot place limits on acceleration due to the companion.

6. Conclusions

We measured flux densities of a sample of X-ray selected low mass stars in the stellar neighborhood. We detected 29 of these stars, consistent with the expectations of the radio-X-ray correlation. Of these stars, we observed 7 with the Very Long Baseline Array and detected 5. Astrometry of these stars indicates that we are not limited by jitter in the stellar position at a level of ~ 0.2 milliarcseconds. Provided that there is not longer-term evolution of the radio activity of these stars, our results indicate that radio-monitoring of these stars can be effective for detection of Jupiter mass planets.

A comparison of radio and optical astrometry allows us to place upper limits on companions. We excluded companions of a ~ 3 to 6 Jupiter masses at a radius of ~ 1 AU for four stars. At radii of 0.3 and 3 AU, limits on companion masses are in the range of 10 to 20 M_J and 20 to 40 M_J , respectively. The short time-baseline of the VLBA measurements limits the acceleration accuracy. Longer time-scale analysis of these sources and others will place much stricter constraints on companion masses.

Additionally, several improvements to observing and analysis methods can improve the quality of results. Due to their large proper motion, some of these stars change position by amounts comparable to or larger than the size of the VLBA synthesized beam during a few hours of observation. Use of data integrated throughout an entire interferometric track thus results in degraded image quality and astrometry. We made a first-order attempt to correct this by splitting some observations into two segments and analyzing them independently; however, more sophisticated approaches in the visibility domain will generate higher quality results. Accurate handling of known orbits for binary stars is also necessary to achieve full sensitivity to planetary companions. Fortunately, known binary companions have periods

that are long compared to the observing period and so residuals are likely to appear as linear terms that can be removed through proper motion fitting. Further, we have performed a simple analysis of orbital parameters given the limited nature of this data; future modeling must solve for orbital parameters in a more complete and thorough manner. Finally, greater sensitivity through increased recording bandwidth and the use of larger apertures can increase SNR and push astrometry accuracy to 0.1 milliarcseconds and smaller.

This paper is the first result from the VLBA+GBT Radio Interferometric Planetary (RIPL) survey. Future papers will investigate the detectability of other stars at high angular resolution, the long-term stability of stellar positions, and the detection of planets through astrometric means.

We thank Jason Wright for generously sharing data that helped define the RIPL target sample. We wish to thank Andrew Howard and Stephen White for their useful comments. The National Radio Astronomy Observatory is a facility of the National Science Foundation operated under cooperative agreement by Associated Universities, Inc. This research has made use of the NASA/IPAC Extragalactic Database (NED) which is operated by the Jet Propulsion Laboratory, California Institute of Technology, under contract with the National Aeronautics and Space Administration. This research has made use of the SIMBAD database, operated at CDS, Strasbourg, France.

REFERENCES

- Bailey, J., Butler, R. P., Tinney, C. G., Jones, H. R. A., O’Toole, S., Carter, B. D., & Marcy, G. W. 2009, *ApJ*, 690, 743
- Beatty, T. G. et al. 2007, *ApJ*, 663, 573
- Beaulieu, J.-P. et al. 2006, *Nature*, 439, 437
- Benedict, G. F. et al. 2002, *ApJ*, 581, L115
- Bennett, D. P. et al. 2008, *ApJ*, 684, 663
- Benz, A. O., & Aref, W. 1991, *A&A*, 252, L19
- Benz, A. O., Aref, W., & Guedel, M. 1995, *A&A*, 298, 187
- Benz, A. O., Conway, J., & Gudel, M. 1998, *A&A*, 331, 596
- Berger, E. 2006, *ApJ*, 648, 629

- Boboltz, D. A., Fey, A. L., Puatua, W. K., Zacharias, N., Claussen, M. J., Johnston, K. J., & Gaume, R. A. 2007, *AJ*, 133, 906
- Boss, A. P. 2006, *ApJ*, 643, 501
- Bower, G. C., Bolatto, A., Ford, E., Kalas, P., & Ulvestad, J. 2007, ArXiv e-prints
- Bower, G. C., Plambeck, R. L., Bolatto, A., McCrady, N., Graham, J. R., de Pater, I., Liu, M. C., & Baganoff, F. K. 2003, *ApJ*, 598, 1140
- Brisken, W. F., Benson, J. M., Goss, W. M., & Thorsett, S. E. 2002, *ApJ*, 571, 906
- Butler, R. P., Johnson, J. A., Marcy, G. W., Wright, J. T., Vogt, S. S., & Fischer, D. A. 2006a, *PASP*, 118, 1685
- Butler, R. P., Vogt, S. S., Marcy, G. W., Fischer, D. A., Wright, J. T., Henry, G. W., Laughlin, G., & Lissauer, J. J. 2004, *ApJ*, 617, 580
- Butler, R. P. et al. 2006b, *ApJ*, 646, 505
- Campbell, B., Walker, G. A. H., & Yang, S. 1988, *ApJ*, 331, 902
- Chauvin, G., Lagrange, A.-M., Dumas, C., Zuckerman, B., Mouillet, D., Song, I., Beuzit, J.-L., & Lowrance, P. 2004, *A&A*, 425, L29
- Chauvin, G. et al. 2005, *A&A*, 438, L29
- Cumming, A., Butler, R. P., Marcy, G. W., Vogt, S. S., Wright, J. T., & Fischer, D. A. 2008, *PASP*, 120, 531
- Cumming, A., Marcy, G. W., & Butler, R. P. 1999, *ApJ*, 526, 890
- Dong, S. et al. 2008, ArXiv e-prints
- Dougherty, S. M., Beasley, A. J., Claussen, M. J., Zauderer, B. A., & Bolingbroke, N. J. 2005, *ApJ*, 623, 447
- Endl, M., Cochran, W. D., Kürster, M., Paulson, D. B., Wittenmyer, R. A., MacQueen, P. J., & Tull, R. G. 2006, *ApJ*, 649, 436
- Fey, A. L. et al. 2004, *AJ*, 127, 3587
- Fomalont, E. B., & Kopeikin, S. M. 2003, *ApJ*, 598, 704
- Forveille, T. et al. 2009, *A&A*, 493, 645

- Gary, D. E., & Linsky, J. L. 1981, *ApJ*, 250, 284
- Gaudi, B. S. et al. 2008, *Science*, 319, 927
- Ge, J., McDavitt, D., Zhao, B., & Miller, S. 2006, in *Society of Photo-Optical Instrumentation Engineers (SPIE) Conference Series*, Vol. 6273, *Society of Photo-Optical Instrumentation Engineers (SPIE) Conference Series*
- Geyer, D. W., Harrington, R. S., & Worley, C. E. 1988, *AJ*, 95, 1841
- Gould, A. et al. 2006, *ApJ*, 644, L37
- Greaves, J. S. et al. 1998, *ApJ*, 506, L133
- Greisen, E. W. 2003, in *Astrophysics and Space Science Library*, Vol. 285, *Astrophysics and Space Science Library*, ed. A. Heck, 109–+
- Güdel, M. 2002, *ARA&A*, 40, 217
- Guirado, J. C. et al. 2006, *A&A*, 446, 733
- Ida, S., & Lin, D. N. C. 2005, *ApJ*, 626, 1045
- Irwin, J., Charbonneau, D., Nutzman, P., & Falco, E. 2009, in *IAU Symposium*, Vol. 253, *IAU Symposium*, 37–43
- Jackson, P. D., Kundu, M. R., & White, S. M. 1987, *ApJ*, 316, L85
- Joergens, V. 2006, *A&A*, 446, 1165
- Johnson, J. A., Butler, R. P., Marcy, G. W., Fischer, D. A., Vogt, S. S., Wright, J. T., & Peek, K. M. G. 2007, *ApJ*, 670, 833
- Kalas, P., Liu, M. C., & Matthews, B. C. 2004, *Science*, 303, 1990
- Kennedy, G. M., Kenyon, S. J., & Bromley, B. C. 2007, *Ap&SS*, 311, 9
- Laughlin, G., Bodenheimer, P., & Adams, F. C. 2004, *ApJ*, 612, L73
- Laughlin, G., Butler, R. P., Fischer, D. A., Marcy, G. W., Vogt, S. S., & Wolf, A. S. 2005, *ApJ*, 622, 1182
- Lépine, S., & Shara, M. M. 2005, *AJ*, 129, 1483
- Lestrade, J.-F., Preston, R. A., Jones, D. L., Phillips, R. B., Rogers, A. E. E., Titus, M. A., Rioja, M. J., & Gabuzda, D. C. 1999, *A&A*, 344, 1014

- Linsky, J. L., & Gary, D. E. 1983, *ApJ*, 274, 776
- Lloyd, J. P. et al. 2009, in *IAU Symposium*, Vol. 253, *IAU Symposium*, 157–161
- Loinard, L., Torres, R. M., Mioduszewski, A. J., Rodríguez, L. F., González-Lópezlira, R. A., Lachaume, R., Vázquez, V., & González, E. 2007, *ApJ*, 671, 546
- Menten, K. M., Reid, M. J., Forbrich, J., & Brunthaler, A. 2007, *A&A*, 474, 515
- Neuhäuser, R., Guenther, E. W., Wuchterl, G., Mugrauer, M., Bedalov, A., & Hauschildt, P. H. 2005, *A&A*, 435, L13
- Pallavicini, R., Willson, R. F., & Lang, K. R. 1985, *A&A*, 149, 95
- Perryman, M. A. C. et al. 1997, *A&A*, 323, L49
- Pestalozzi, M. R., Benz, A. O., Conway, J. E., & Güdel, M. 2000, *A&A*, 353, 569
- Phillips, R. B., Lonsdale, C. J., Feigelson, E. D., & Deeney, B. D. 1996, *AJ*, 111, 918
- Pravdo, S. H., & Shaklan, S. B. 1996, *ApJ*, 465, 264
- Pravdo, S. H., & Shaklan, S. B. 2003, in *Astronomical Society of the Pacific Conference Series*, Vol. 294, *Scientific Frontiers in Research on Extrasolar Planets*, ed. D. Deming & S. Seager, 107–110
- Pravdo, S. H., Shaklan, S. B., & Lloyd, J. 2005, *ApJ*, 630, 528
- Ramsey, L. W., Barnes, J., Redman, S. L., Jones, H. R. A., Wolszczan, A., Bongiorno, S., Engel, L., & Jenkins, J. 2008, *PASP*, 120, 887
- Reid, M. J., & Brunthaler, A. 2004, *ApJ*, 616, 872
- Rivera, E. J. et al. 2005, *ApJ*, 634, 625
- Salim, S., & Gould, A. 2003, *ApJ*, 582, 1011
- Sandstrom, K. M., Peek, J. E. G., Bower, G. C., Bolatto, A. D., & Plambeck, R. L. 2007, *ApJ*, 667, 1161
- Schmitt, J. H. M. M., & Liefke, C. 2004, *A&A*, 417, 651
- Shao, M., & Nemati, B. 2009, *PASP*, 121, 41
- Udalski, A. et al. 2005, *ApJ*, 628, L109

White, S. M., Lim, J., & Kundu, M. R. 1994, ApJ, 422, 293

Wright, J. T. 2005, PASP, 117, 657

Xu, Y., Reid, M. J., Menten, K. M., Brunthaler, A., Zheng, X. W., & Moscadelli, L. 2009, ApJ, 693, 413

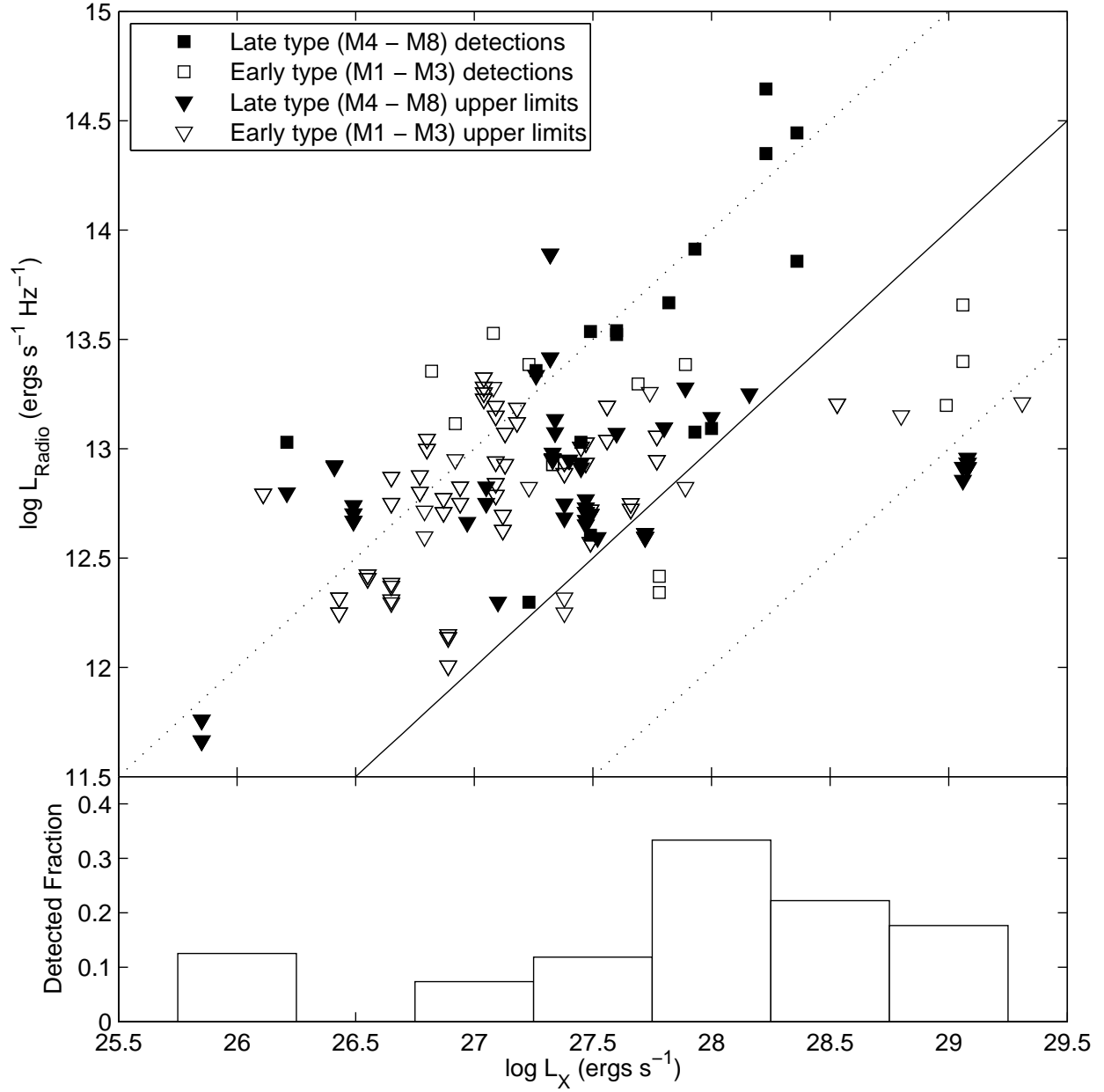


Fig. 1.— Radio and X-ray luminosities. Results are plotted separately for late type (filled symbols) and early type (unfilled symbols), where the dividing spectral type is M4. Squares represent detections and triangles represent upper limits. The solid line is the nominal correlation $L_R = 10^{-15} L_X$ Hz. Dashed lines represent the standard uncertainty of an order of magnitude in the scale factor. A histogram of detected fraction as a function of L_X is also given.

Table 1. Stellar Data

GJ	RA (J2000)	Dec (J2000)	Pos. Err (mas,mas,deg)	PM $_{\alpha}$,PM $_{\delta}$ (mas/yr)	PM $_{err}$ (mas/yr,mas/yr,deg)	Π (mas)	Π_{err} (mas)	Sp	m $_B$	m $_V$	Log L $_X$ (erg s $^{-1}$)
1005A	00 15 27.70	-16 -7 -56.00	191.80	0.00	M4	...	13.29	26.21
15A	00 18 22.89	44 01 22.63	06.48,05.55, 73	2888.70, 410.21	0.75, 0.63, 79	280.20	1.05	M1.5V	9.63	8.07	26.43
15B	00 18 25.81	44 01 38.00	...	2876.00, 341.00	5.00, 5.00, 97	280.20	0.00	M3.5	12.84	11.04	27.38
2005B	00 24 44.21	-27 -8 -24.40	135.30	0.00	M8.5V	27.32
2005C	00 24 44.21	-27 -8 -24.40	135.30	0.00	M9V	27.32
48	01 02 32.23	71 40 47.34	11.19,08.66, 131	1745.50, -380.80	1.25, 0.99, 135	122.70	1.23	M3.5V:e	11.42	9.96	26.80
53B	01 08 16.40	54 55 13.00	...	3420.00, -1600.00	...	132.40	0.00	sdM	...	11.10	26.82
3076	01 11 25.42	15 26 21.90	...	185.00, -121.00	5.00, 5.00, 90	M5	...	13.59	27.70
54.1	01 12 30.64	-16 -59 -56.28	50.02,21.33, 58	1209.90, 646.88	5.93, 2.70, 57	269.00	7.57	M4.5	12.80	11.60	27.40
65A	01 39 01.54	-17 -57 -1.80	...	3296.00, 563.00	5.00, 5.00, 142	373.70	0.00	M5.5V:e	14.42	12.57	27.60
65B	01 39 01.54	-17 -57 -1.80	...	3296.00, 563.00	5.00, 5.00, 142	381.00	6.00	M5.5e	14.37	12.52	27.60
83.1	02 00 12.96	13 03 06.70	...	1091.00, -1780.00	5.00, 5.00, 45	222.00	5.00	M4.5	14.08	12.26	27.38
3125	02 01 54.08	73 32 32.00	...	276.00, -112.00	5.00, 5.00, 90	M4.5	16.02	14.12	27.47
84	02 05 04.85	-17 -36 -52.67	16.44,10.73, 63	1317.50, -173.90	1.86, 1.21, 62	105.90	2.04	M2.5	11.71	10.19	27.69
3146	02 16 29.85	13 35 12.70	...	501.00, -437.00	5.00, 5.00, 58	118.20	6.80	M5.5	17.77	15.79	27.26
102	02 33 37.18	24 55 37.60	...	51.00, -679.00	5.00, 5.00, 77	129.00	12.00	M4	14.66	12.96	28.00
105C	02 35 58.80	06 52 01.00	3000.00,3000.00, 45	138.70	0.00	M6V	27.34
109	02 44 15.51	25 31 24.08	21.56,14.24, 100	864.67, -367.10	2.39, 1.66, 99	132.40	2.48	M3	12.13	10.58	27.33
3193B	03 01 51.42	-16 -35 -36.13	...	-343.00, -291.00	2.00, 2.00, 90	M3	...	11.30	27.88
144.0	03 32 55.84	-9 -27 -29.74	09.48,06.79, 53	-976.30, 17.98	1.09, 0.77, 49	310.70	0.85	K2V	4.61	3.73	...
166C	04 15 21.50	-7 -39 -22.30	...	-2239.00, -3419.00	...	198.20	0.00	M4.5	12.85	11.17	28.16
169.1A	04 31 11.52	58 58 37.46	...	1300.00, -2049.00	4.00, 3.00, 0	178.00	2.00	M4	12.73	11.08	26.41
3304	04 38 12.61	28 13 00.40	...	385.00, -80.00	5.00, 5.00, 27	M4	14.16	12.51	28.34
176	04 42 55.78	18 57 29.42	29.29,13.32, 62	659.78, -1114.00	3.45, 1.48, 61	106.10	2.51	K5	11.48	9.97	...
3323	05 01 57.43	-6 -56 -46.50	...	-550.00, -533.00	5.00, 5.00, 90	163.00	0.00	M4	13.92	12.16	27.48
185B	05 02 28.42	-21 -15 -23.90	129.40	0.00	M2V	27.12
190	05 08 35.05	-18 -10 -19.37	13.47,09.72, 153	503.76, -1400.00	1.52, 1.15, 152	107.30	2.00	M3.5	11.83	10.31	27.28
205	05 31 27.40	-3 -40 -38.02	10.23,06.46, 81	763.03, -2092.00	1.16, 0.72, 79	175.70	1.20	M1.5V	9.44	7.92	27.66
213	05 42 09.27	12 29 21.62	22.77,13.49, 89	1998.30, -1570.00	2.67, 1.67, 88	172.70	3.88	M4V	13.15	11.48	27.64
3379	06 00 03.49	02 42 23.67	...	311.00, -42.00	2.00, 2.00, 0	186.30	6.20	M3.5V	13.01	11.33	27.92
226	06 10 19.85	82 06 24.31	11.60,09.65, 47	50.24, -1336.00	1.34, 1.11, 46	106.40	1.44	M2	12.00	10.49	27.09
229A	06 10 34.62	-21 -51 -52.72	08.24,04.82, 156	-137.00, -714.00	0.93, 0.54, 158	173.10	1.12	M1/M2V	9.65	8.14	27.11
234A	06 29 23.40	-2 -48 -50.32	28.81,15.90, 55	694.66, -618.50	3.43, 1.84, 53	242.80	2.64	M4.5	13.08	11.10	27.97
234B	06 29 23.52	-2 -48 -51.10	2000.00,2000.00, 45	707.00, -703.00	...	242.80	0.00	M8V	16.00	14.60	27.97

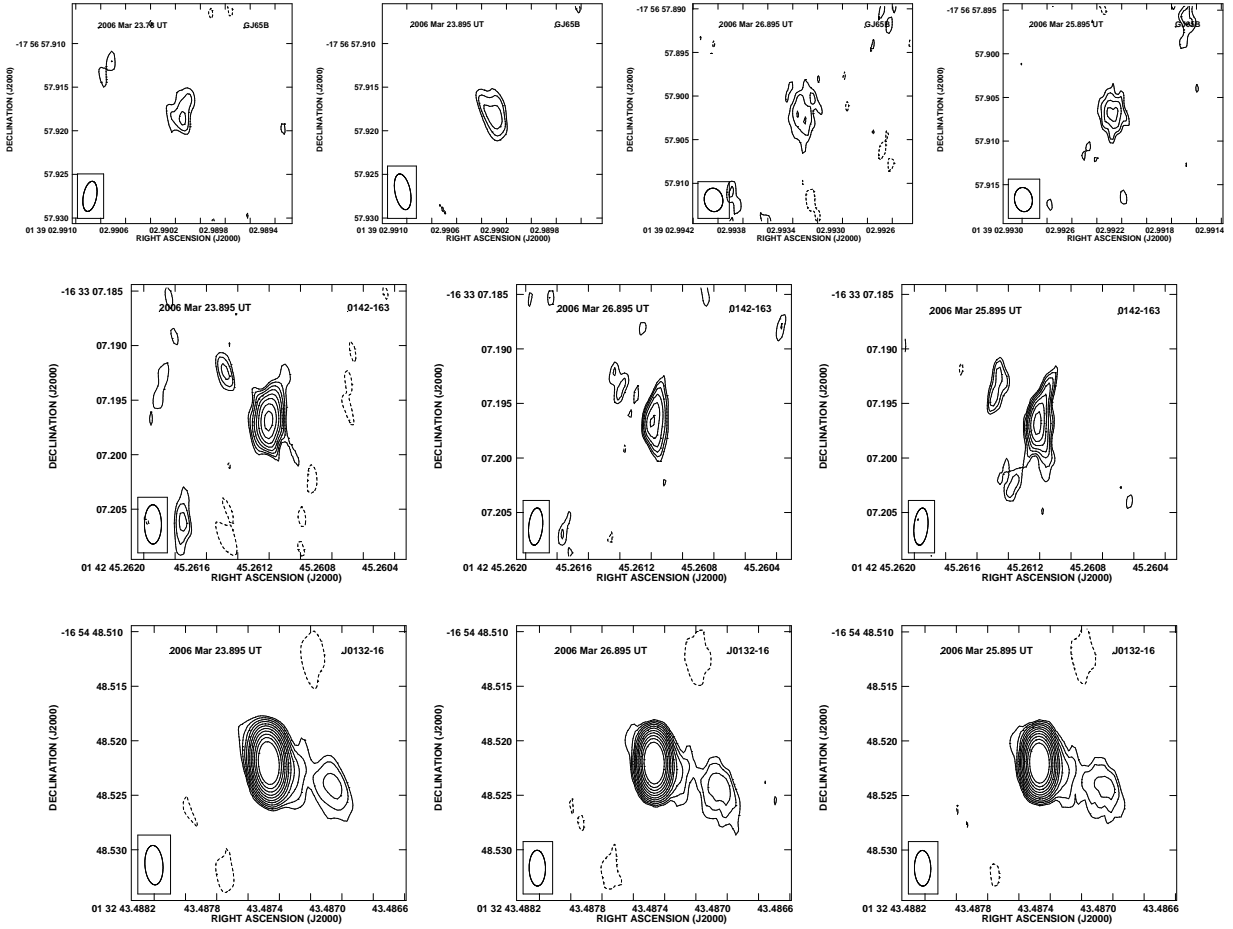


Fig. 2.— Images of GJ 65B and its calibrators J0142-1633 (secondary) and J0132-16 (primary) from all observing epochs. Two images of GJ65B from the first and second half of the first epoch are shown. Contours are -3, 3, 4.2, 6, 8.4, 12, 16.8 times the image rms noise for the star and the secondary calibrator. Contours are -5, 5, 7, 10, 14, ..., 160 times the image rms noise for the primary calibrators. The synthesized beam is shown in the lower left. The epoch is written in the upper left.

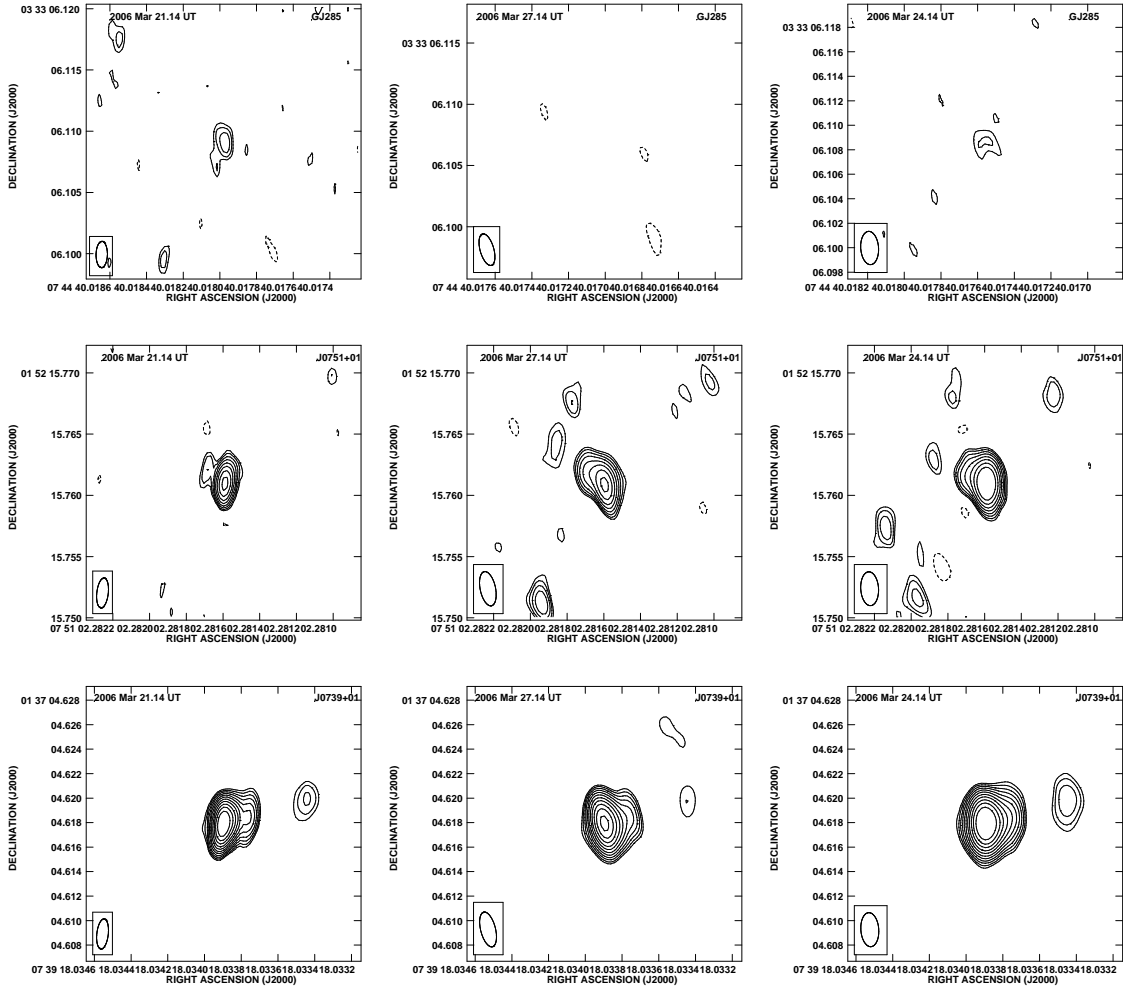


Fig. 3.— Images of GJ 285 and its calibrators J0751+152 (secondary) and J0739+0137 (primary). Contours and labels are as described for Figure 3.

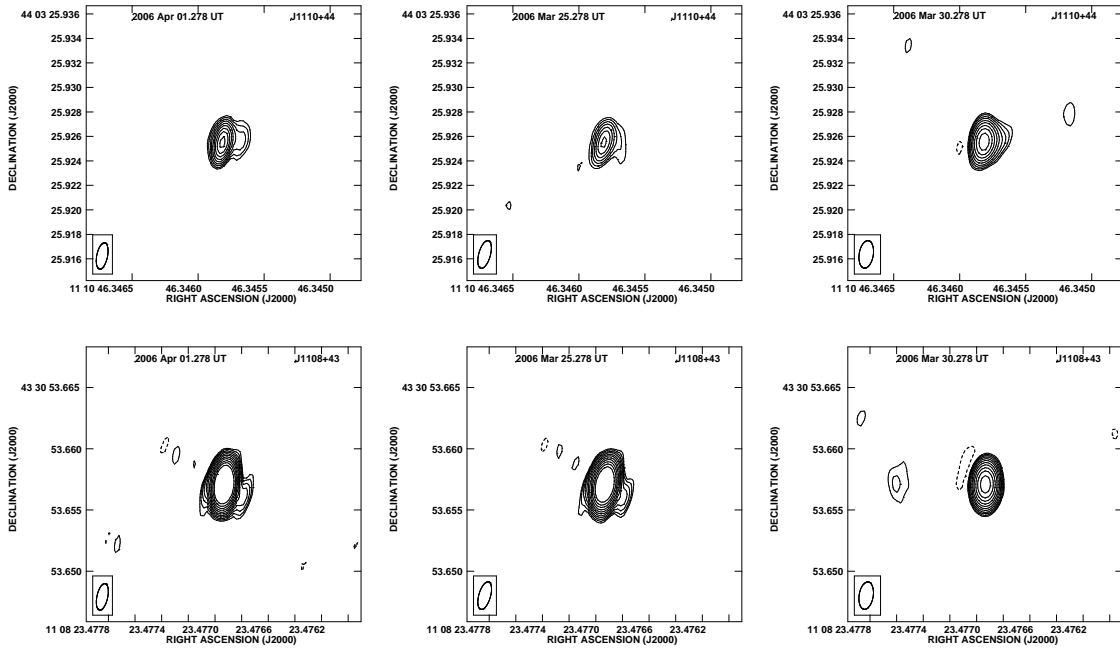


Fig. 4.— Images of the calibrators for GJ 412B: J1110+4403 (secondary) and J1108+4330 (primary). Contours and labels are as described for Figure 2.

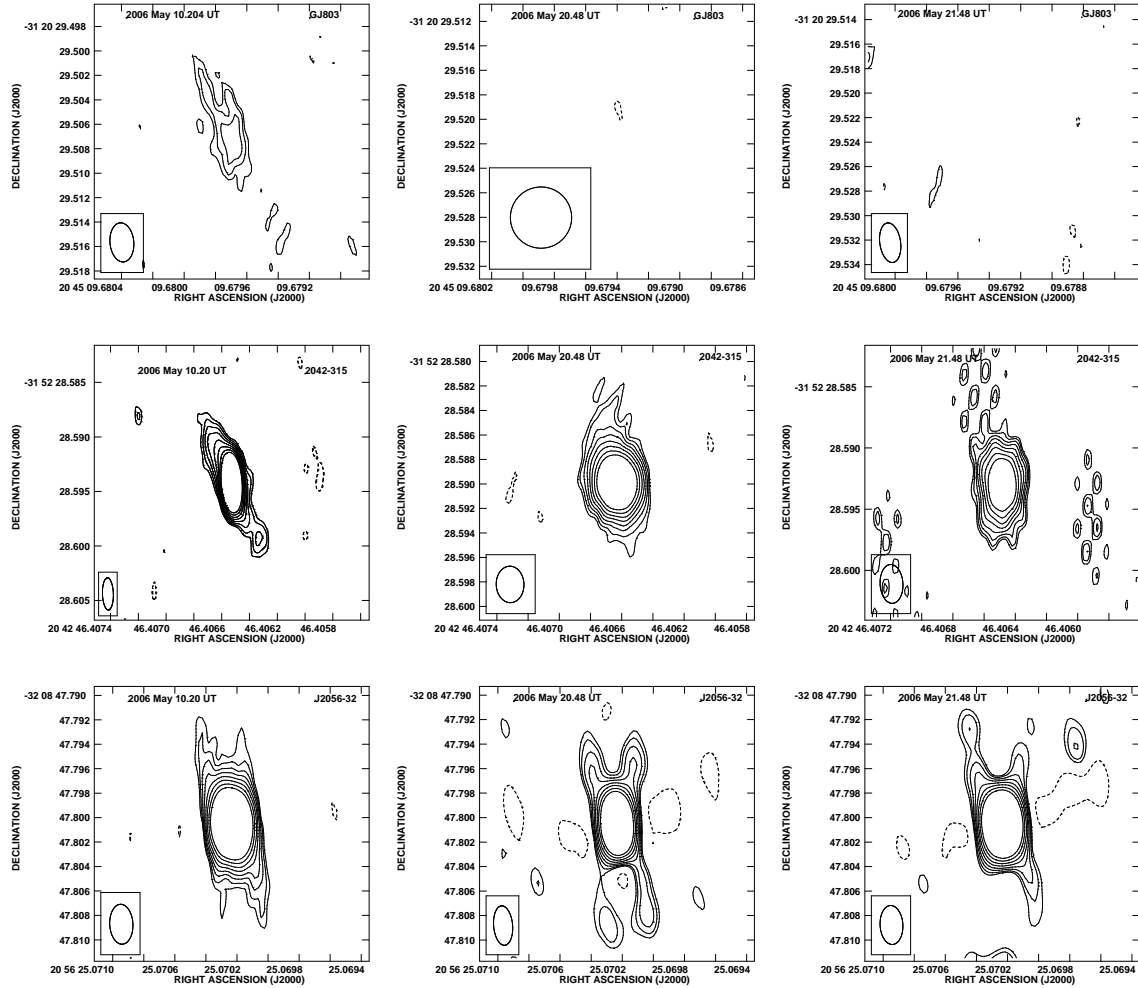


Fig. 5.— Images of GJ 803 and its calibrators J2042-3152 (secondary) and J2056-3208 (primary). Contours and labels are as described for Figure 2.

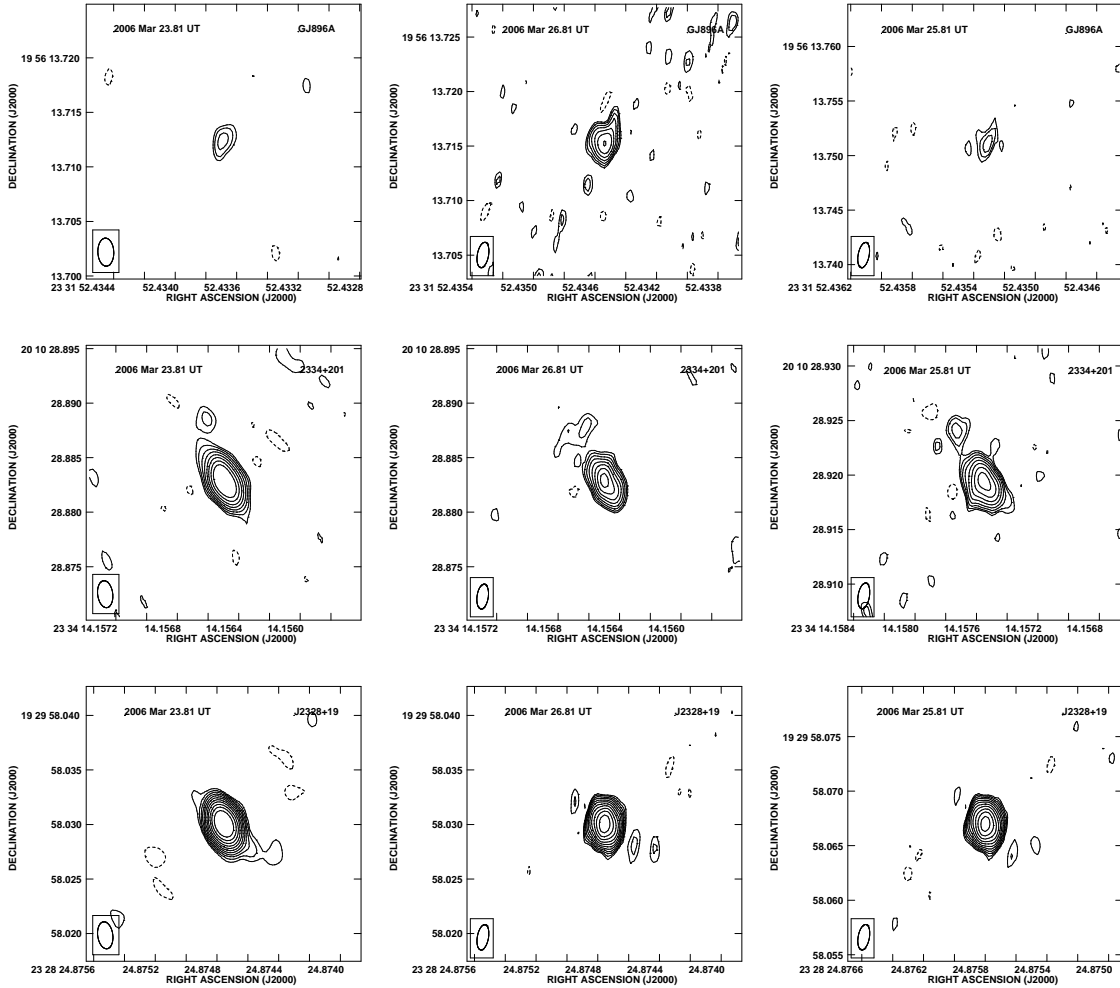


Fig. 6.— Images of GJ 896 and its calibrators J2334+2010 (secondary) and J2328+1929 (primary). Contours and labels are as described for Figure 2.

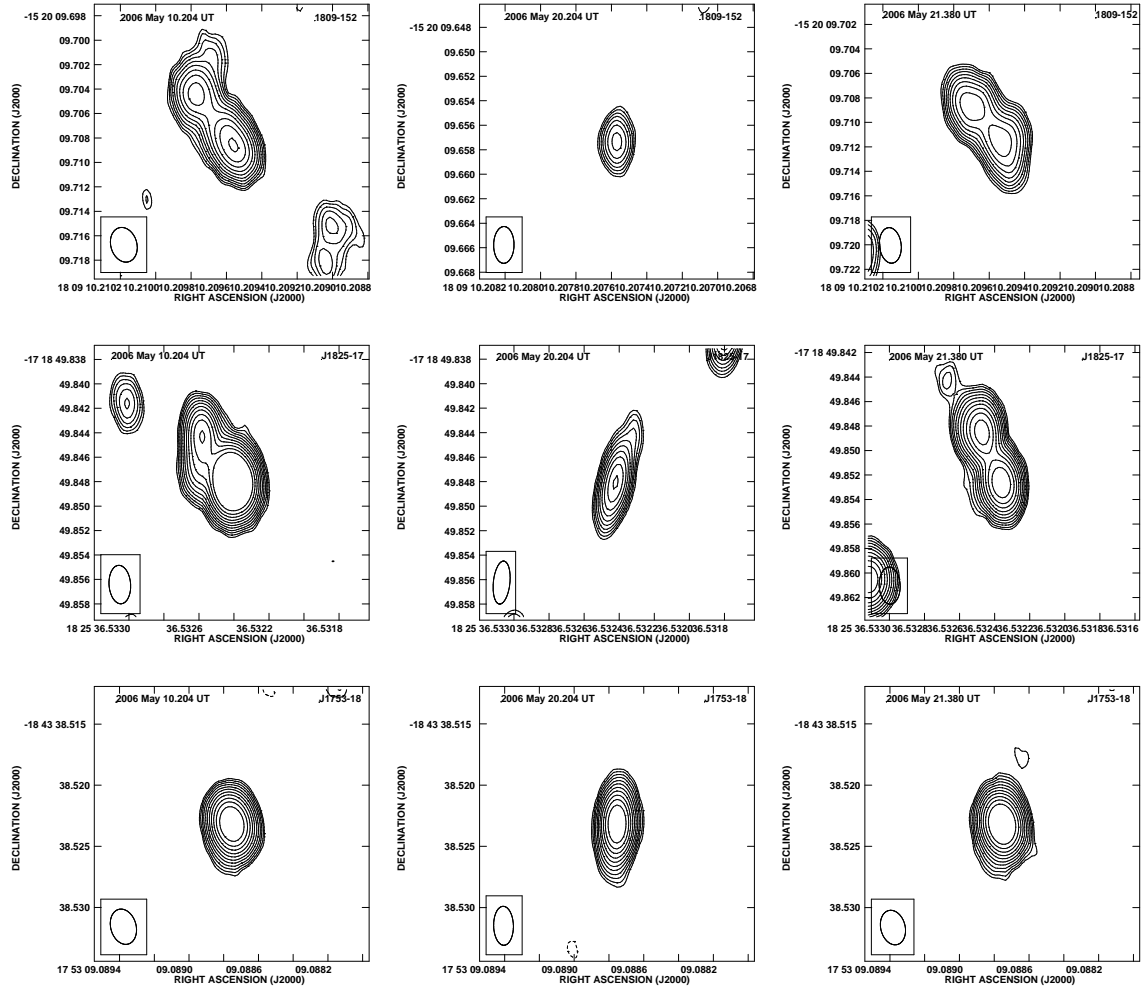


Fig. 7.— Images of the calibrators for GJ 1224: J1809-1520 and J1825-1718 (secondary) and J1753-1843 (primary). Contours and labels are as described for Figure 2.

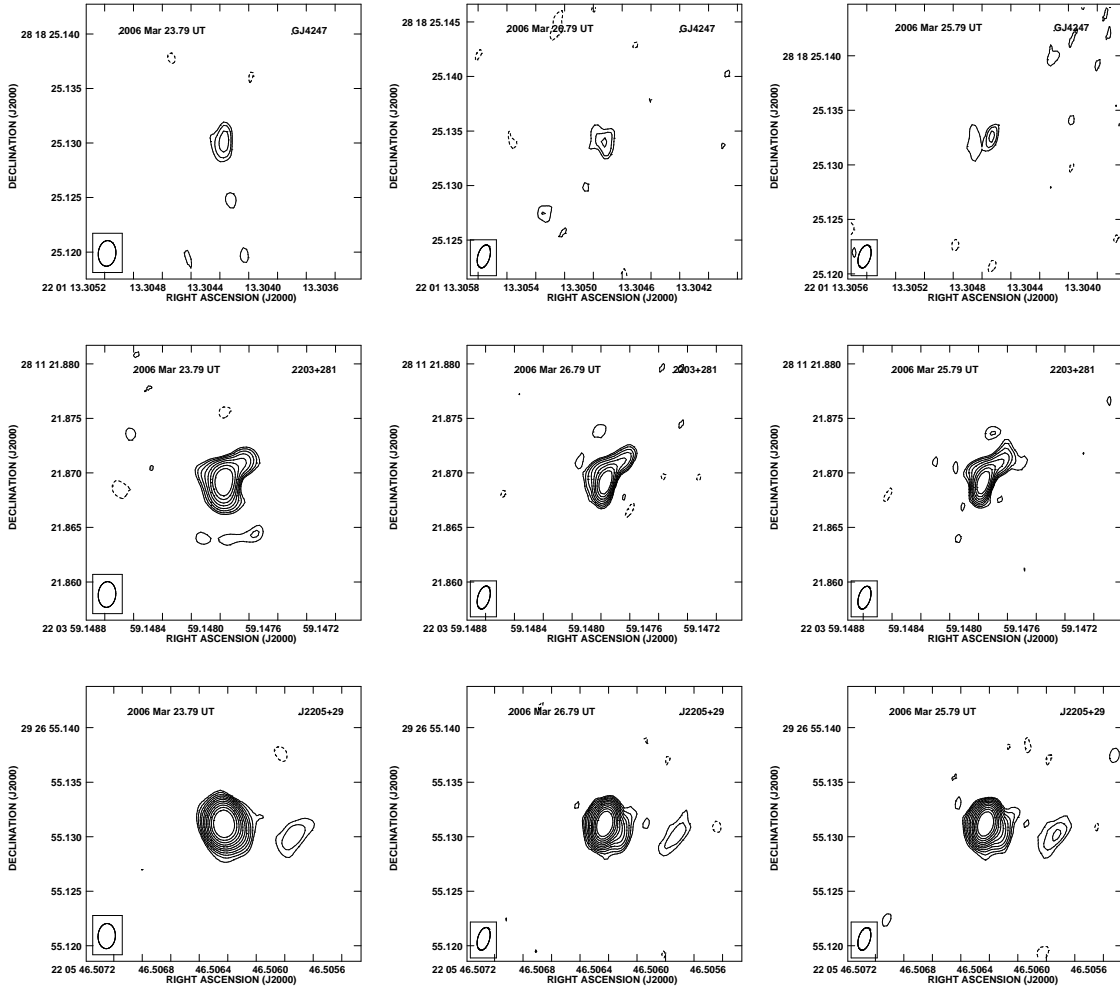


Fig. 8.— Images of GJ 4247 and its calibrators J2203+281 (secondary) and J2205+2926 (primary). Contours and labels are as described for Figure 2.

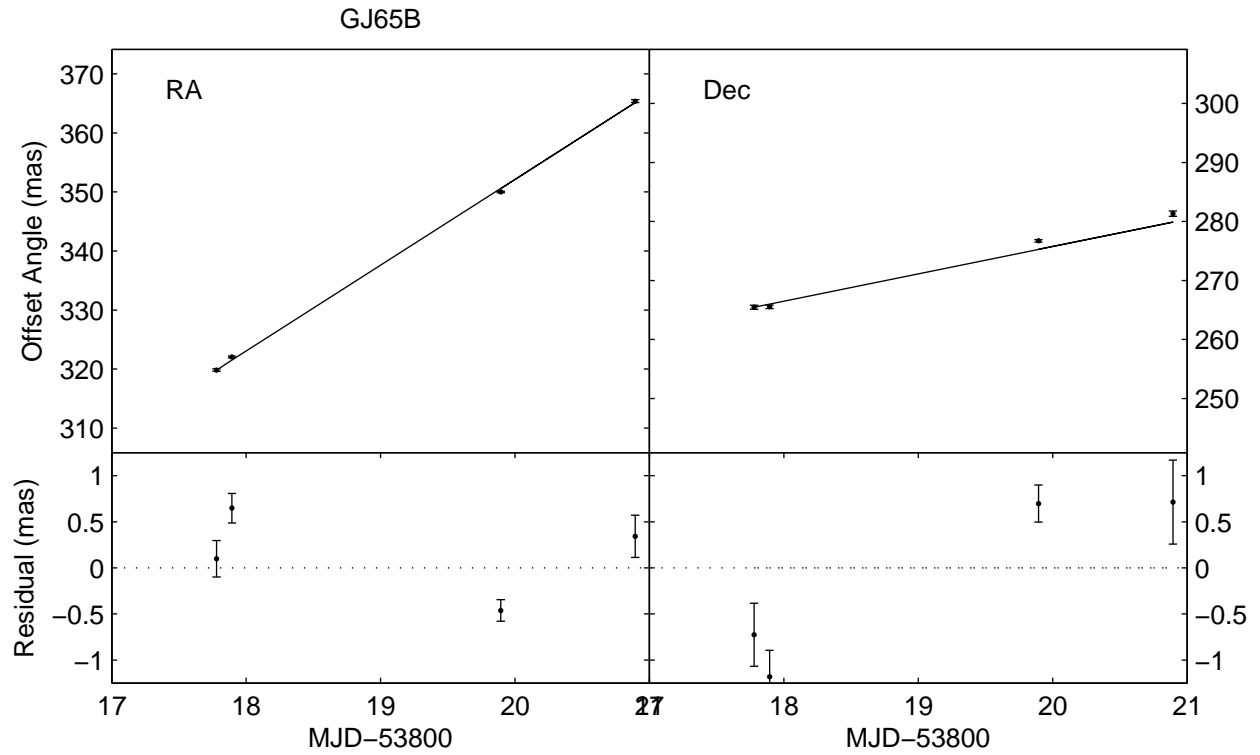


Fig. 9.— Motion of GJ 65B in RA and Dec. Plotted radio positions are relative to optical position at first epoch. The solid line shows the predicted optical position due to parallax and proper motion. The lower panels show the residual after removal of the optical predictions and the mean offset between radio and optical.

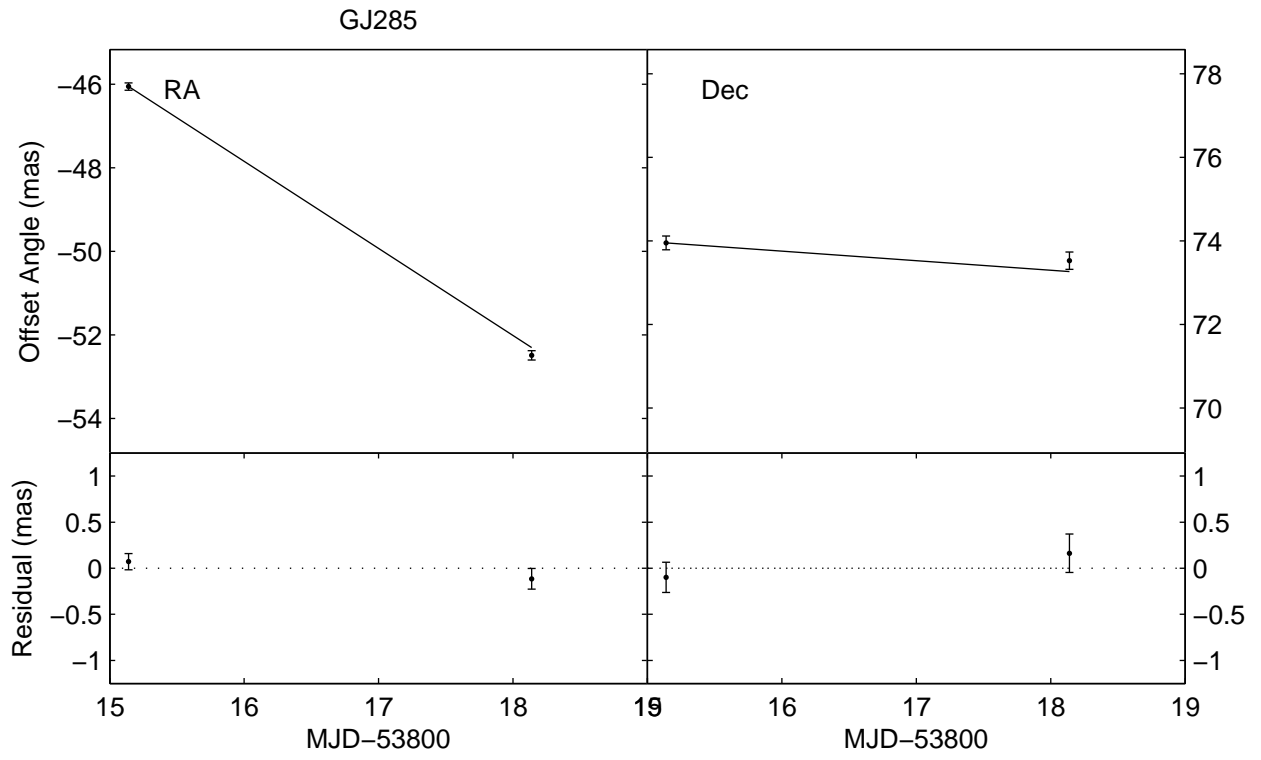


Fig. 10.— Motion of GJ 285. See Figure 9 for details.

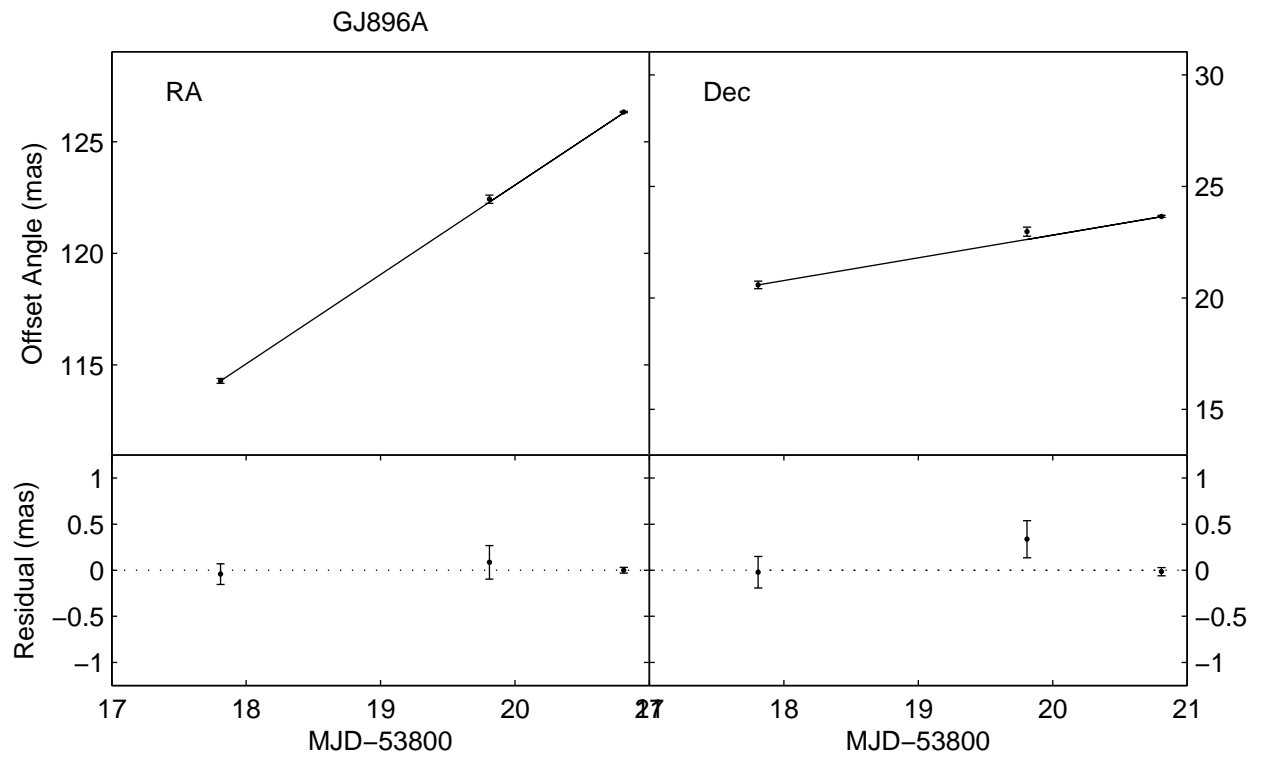


Fig. 11.— Motion of GJ 896A. See Figure 9 for details.

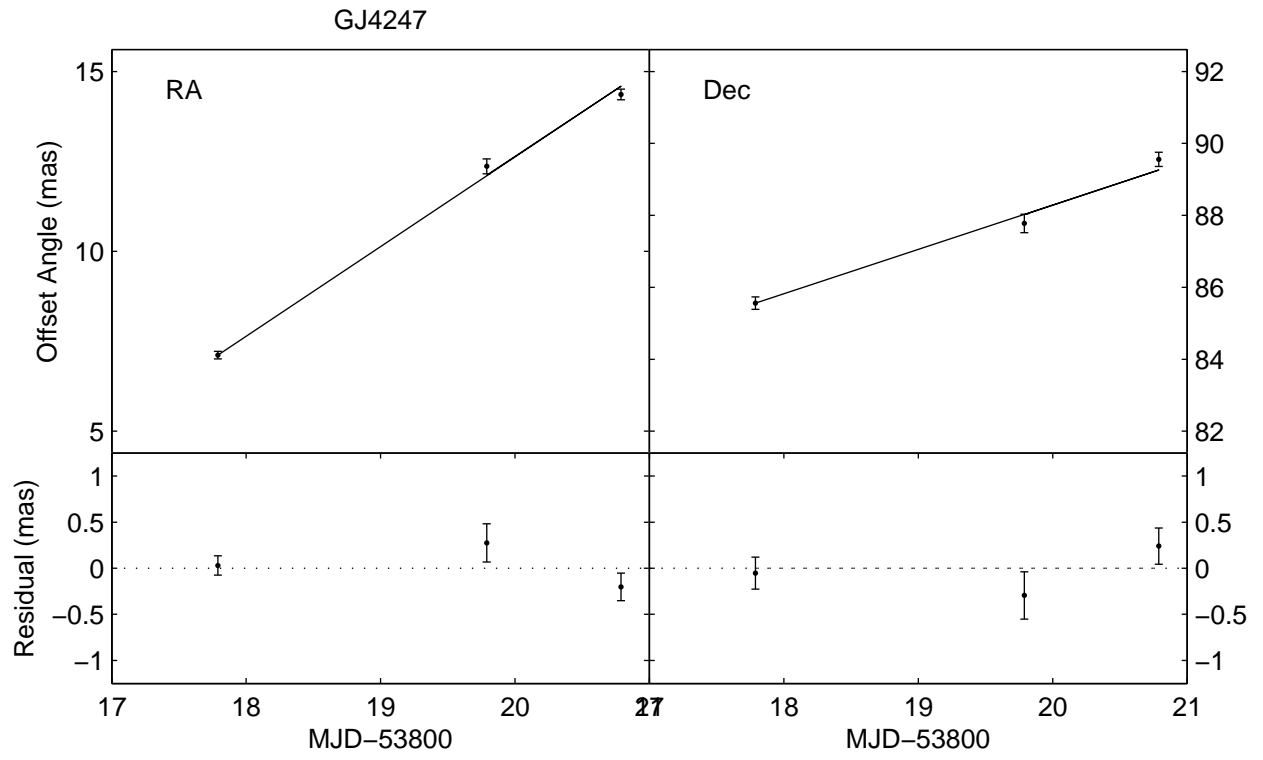


Fig. 12.— Motion of GJ 4247. See Figure 9 for details.

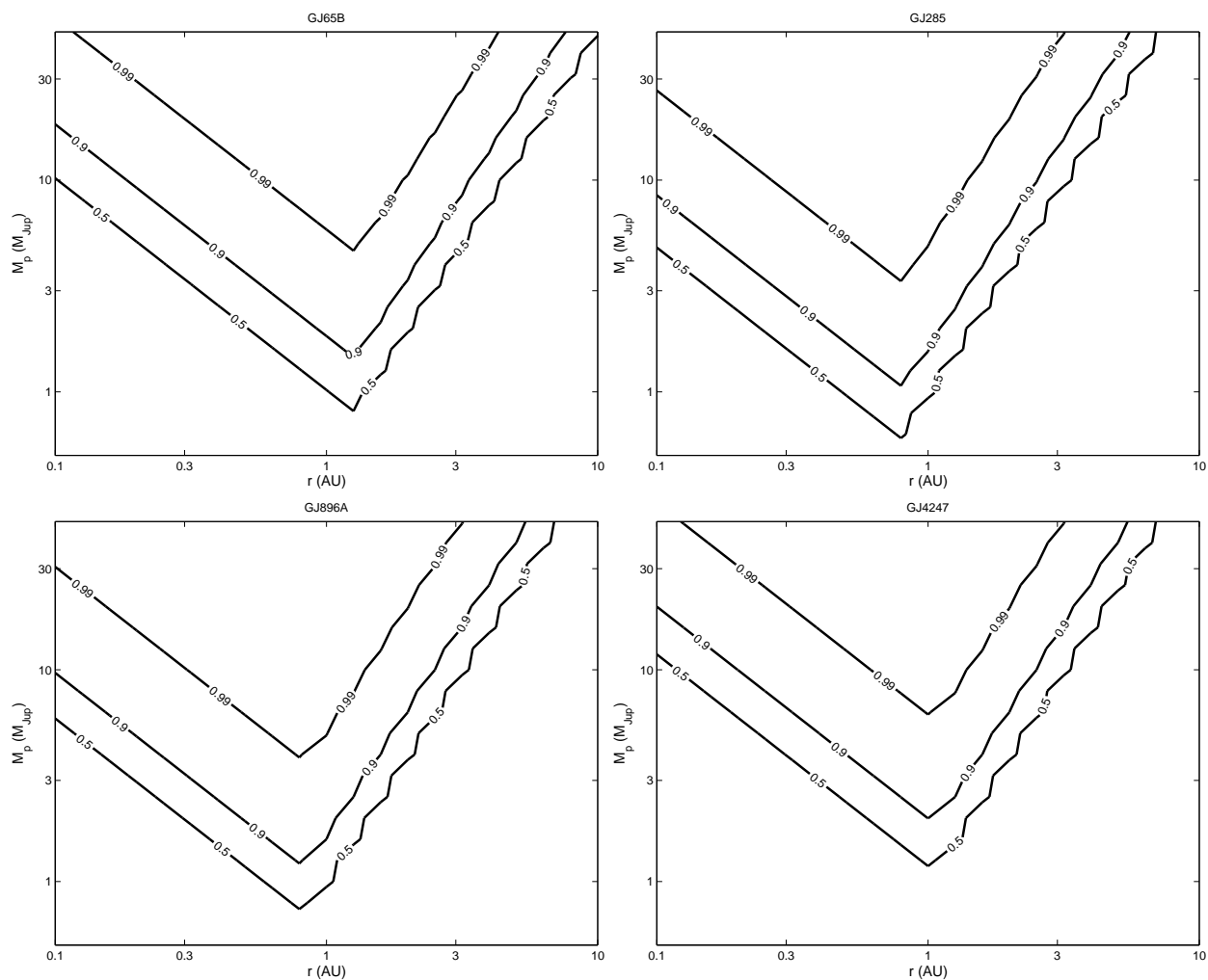


Fig. 13.— Region of planetary mass and radius phase-space rejected by acceleration upper limits. Contours are for parameters for which 99%, 90%, 50%, and 10% of systems would be detected with 3σ confidence. Parameter space above the curves is rejected. Wiggles in the curves are due to logarithmic gridding of the model.

Table 1—Continued

GJ	RA (J2000)	Dec (J2000)	Pos. Err (mas,mas,deg)	PM $_{\alpha}$,PM $_{\delta}$ (mas/yr)	PM $_{err}$ (mas/yr,mas/yr,deg)	Π (mas)	Π_{err} (mas)	Sp	m $_B$	m $_V$	Log L $_X$ (erg s $^{-1}$)
250B	06 52 18.07	-5 -11 -25.60	2000.00,2000.00, 89	-541.00, 0.00	..., ...,	M2	11.47	10.05	28.10
251	06 54 48.96	33 16 05.43	18.67,10.28, 72	-729.20, -399.20	2.13, 1.21, 70	181.30	1.87	M3	11.47	9.89	26.11
268A	07 10 01.83	38 31 46.06	46.84,22.32, 80	-439.60, -948.20	5.40, 2.63, 78	157.20	3.32	M4.5	13.19	11.47	27.87
273	07 27 24.50	05 13 32.83	12.10,07.20, 103	571.26, -3694.00	1.43, 0.87, 102	263.20	1.43	M3.5	11.42	9.89	26.55
285	07 44 40.17	03 33 08.83	22.44,14.81, 98	-344.80, -450.80	2.62, 1.73, 96	168.50	2.67	M4.5V:e	12.73	11.12	28.57
300	08 12 40.87	-21 -33 -6.80	..., ..., ...	9.00, -694.00	5.00, 5.00, 90	166.00	11.00	M4	13.80	13.00	26.26
2066	08 16 07.98	01 18 09.26	18.91,13.34, 89	-375.00, 60.11	2.17, 1.49, 88	109.20	1.79	M2	11.55	10.05	...
1111	08 29 49.35	26 46 33.70	..., ..., ...	-1111.00, -612.00	5.00, 5.00, 152	275.80	0.00	M6	16.87	14.81	26.58
3517	08 53 36.20	-3 -29 -32.10	60.00,60.00, 45	-502.00, -211.00	5.00, 5.00, 4	116.80	1.50	M9V	20.80	20.80	26.67
1116A	08 58 15.19	19 45 47.10	70.00,60.00, 0	-846.00, -65.00	5.00, 5.00, 0	190.00	3.00	M8Ve	15.90	14.06	27.82
1116B	08 58 15.13	19 45 47.10	..., ..., ...	-846.00, -65.00	5.00, 5.00, 0	190.00	5.00	M5.5	16.85	14.92	27.82
3522	08 58 56.45	08 28 24.60	2000.00,2000.00, 97	410.00, -367.00	100.00, 100.00, 90	M3.5	12.57	10.89	28.65
338A	09 14 22.79	52 41 11.85	57.93,32.48, 91	-1533.00, -562.90	6.80, 3.97, 91	161.50	5.23	M0V	9.07	7.64	...
382	10 12 17.67	-3 -44 -44.38	11.74,07.96, 118	-152.90, -242.80	1.38, 0.93, 116	127.90	1.53	M1.5	10.77	9.26	27.45
388	10 19 36.27	19 52 11.90	137.63,133.11, 90	-500.80, -46.00	2.00, 1.90, 88	213.00	4.00	M3.5V	10.97	9.43	28.80
393	10 28 55.55	00 50 27.60	20.08,11.93, 136	-602.30, -731.80	2.49, 1.37, 139	138.20	2.13	M2	11.15	9.63	...
3622	10 48 12.61	-11 -20 -9.70	..., ..., ...	580.00, -1531.00	5.00, 5.00, 122	221.00	3.60	M6.5	17.70	15.60	25.96
406	10 56 28.99	07 00 52.00	2000.00,2000.00, 0	-3842.00, -2725.00	100.00, 100.00, 1	425.00	7.00	M5.5V	15.54	13.54	26.97
408	11 00 04.26	22 49 58.67	14.22,08.99, 90	-426.20, -279.90	1.69, 1.04, 85	150.90	1.59	M2.5	11.58	10.03	...
411	11 03 20.19	35 58 11.55	08.43,04.71, 134	-580.40, -4769.00	0.95, 0.53, 133	392.50	0.91	M2V	9.00	7.49	26.89
412A	11 05 28.58	43 31 36.39	08.89,06.78, 123	-4409.00, 942.31	1.02, 0.77, 127	206.90	1.19	M0.5	10.22	8.68	27.49
412B	11 05 30.90	43 31 17.90	..., ..., ...	-4328.00, 952.00	5.00, 5.00, 90	206.90	0.00	M6	16.45	14.45	27.49
424	11 20 04.83	65 50 47.35	08.82,07.38, 111	-2946.00, 183.68	1.00, 0.86, 112	109.90	1.11	M0	10.74	9.32	27.04
436	11 42 11.09	26 42 23.65	25.12,14.95, 80	896.34, -813.70	2.96, 1.79, 80	97.73	2.27	M2.5	12.20	10.68	...
445	11 47 41.38	78 41 28.18	13.54,10.69, 81	743.58, 480.47	1.56, 1.20, 81	185.50	1.43	M3.5	12.37	10.78	26.65
450	11 51 07.34	35 16 19.26	10.81,06.77, 87	-271.90, 254.93	1.30, 0.83, 88	116.90	1.38	M1	11.30	9.78	27.56
451B	11 52 60.00	37 43 00.00	180004.00,180003.00, 55	3995.00, -5806.00	25.00, 25.00, 145	M5.5V	...	12.00	26.49
1156	12 18 59.49	11 07 32.80	2000.00,2000.00, 90	-1246.00, 186.00	100.00, 100.00, 90	152.90	0.00	M5	15.62	13.79	27.60
473A	12 33 16.30	09 01 26.00	..., ...,, ...,, ..., ...	227.90	0.00	M4V	...	12.44	27.52
473B	12 33 19.10	09 01 10.00	3000.00,3000.00, 179	-1744.00, 263.00	25.00, 25.00, 58	227.90	0.00	M7	...	13.40	27.52
486	12 47 56.62	09 45 05.03	26.79,13.07, 111	-1007.00, -461.00	3.03, 1.57, 113	121.70	2.90	M3.5	12.96	11.40	...
493.1	13 00 33.54	05 41 08.50	2000.00,2000.00, 45	-940.00, 241.00	100.00, 100.00, 178	M4.5	15.12	13.37	27.82
504	13 16 46.52	09 25 26.96	07.43,04.09, 111	-334.50, 190.70	0.85, 0.46, 113	55.71	0.85	GOVs	5.81	5.22	...
514	13 29 59.79	10 22 37.78	10.61,06.10, 91	1127.90, -1074.00	1.17, 0.67, 94	131.10	1.29	M0.5	10.54	9.04	27.38

Table 1—Continued

GJ	RA (J2000)	Dec (J2000)	Pos. Err (mas,mas,deg)	PM $_{\alpha}$,PM $_{\delta}$ (mas/yr)	PM $_{err}$ (mas/yr,mas/yr,deg)	Π (mas)	Π_{err} (mas)	Sp	m $_B$	m $_V$	Log L $_X$ (erg s $^{-1}$)
3789	13 31 46.61	29 16 36.69	...	-234.00, -137.00	2.00, 2.00, 90	126.00	0.00	M4	13.52	11.95	28.23
526	13 45 43.78	14 53 29.47	09.87,06.83, 128	1778.30, -1455.00	1.09, 0.75, 127	184.10	1.27	M2V	9.91	8.46	26.87
3820	13 59 10.43	-19 -50 -3.60	...	-552.00, -183.00	5.00, 5.00, 11	M4	14.70	13.00	28.04
557.0	14 34 40.82	29 44 42.47	06.42,04.08, 140	188.32, 132.72	0.73, 0.47, 137	64.66	0.72	F2V	4.82	4.46	...
566A	14 51 23.10	19 06 02.00	3250.00,3250.00, 0	139.00, -99.00	25.00, 25.00, 157	149.20	0.00	G8V	5.40	4.70	...
569B	14 54 29.00	16 06 05.00	M8.5	...	18.10	28.53
569A	14 54 29.24	16 06 03.82	16.58,11.37, 84	275.95, -122.10	1.96, 1.31, 80	101.90	1.67	M2.5V	11.68	10.20	28.53
3877	14 56 38.31	-28 -9 -47.40	60.00,60.00, 17	-497.00, -827.00	5.00, 5.00, 22	157.80	5.10	M5V	18.39	17.05	26.19
570C	14 57 26.50	-21 -24 -41.00	133.60	33.56	M3V	...	9.94	27.74
570B	14 57 26.54	-21 -24 -41.47	404.97,242.74, 99	987.02, -1666.00	44.89, 28.17, 98	133.60	33.56	M1V	9.68	8.10	27.74
581	15 19 26.82	-7 -43 -20.21	27.21,14.51, 77	-1224.00, -99.51	3.13, 1.68, 76	159.50	2.27	M3	12.17	10.56	...
625	16 25 24.62	54 18 14.77	11.85,10.46, 63	432.29, -170.70	1.34, 1.18, 67	151.90	1.11	M1.5	10.89	10.40	26.77
628	16 30 18.06	-12 -39 -45.34	22.31,11.34, 124	-93.62, -1184.00	2.51, 1.25, 123	234.50	1.82	M3.5	11.72	10.12	26.79
638	16 45 06.35	33 30 33.23	07.87,06.41, 173	-39.18, 383.43	0.89, 0.72, 170	102.30	0.88	K5	9.48	8.11	...
643	16 55 25.23	-8 -19 -21.27	39.55,23.03, 84	-813.40, -895.10	4.43, 2.46, 82	153.90	4.04	M3.5	13.40	11.70	29.08
644A	16 55 26.34	-8 -20 -53.90	1285.00,1285.00, 9	-791.00, -878.00	25.00, 25.00, 90	153.90	0.00	M3	11.40	9.80	29.08
644B	16 55 26.34	-8 -20 -53.90	1285.00,1285.00, 9	-791.00, -878.00	25.00, 25.00, 90	153.90	0.00	M4	...	9.80	29.08
644C	16 55 35.29	-8 -23 -40.10	60.00,60.00, 87	-771.00, -871.00	23.00, 21.00, 0	153.90	0.00	M6.5V	18.70	16.70	27.45
1207	16 57 05.80	-4 -20 -57.00	2000.00,2000.00, 45	513.00, -377.00	M3.5	13.92	12.33	28.39
661A	17 12 07.83	45 39 57.68	...	252.00, -1571.00	1.00, 1.00, 72	158.10	0.00	M3.5	11.50	10.00	27.23
661B	17 12 07.83	45 39 57.68	...	252.00, -1571.00	1.00, 1.00, 72	158.10	0.00	M3	11.30	10.30	27.89
673	17 25 45.23	02 06 41.12	07.17,05.06, 81	-580.50, -1184.00	0.81, 0.57, 82	129.50	0.95	K5	8.90	7.54	...
687	17 36 25.90	68 20 20.91	11.63,08.60, 22	-320.40, -1269.00	1.36, 1.02, 21	220.80	0.92	M3	10.65	9.15	...
686	17 37 53.35	18 35 30.15	12.63,09.72, 143	926.84, 983.18	1.42, 1.07, 142	123.00	1.62	M1	11.15	9.62	...
694	17 43 55.96	43 22 43.00	11.96,09.36, 48	9.48, -602.60	1.39, 1.08, 45	105.30	1.15	M2.5	12.05	10.50	27.18
695B	17 46 25.16	27 43 00.74	439.88,425.86, 90	-332.00, -753.00	5.80, 5.60, 90	M3.5	11.27	9.78	28.00
695C	17 46 25.20	27 43 01.00	...	-301.00, -750.00	25.00, 25.00, 0	M4	...	10.80	28.00
699	17 57 48.50	04 41 36.25	14.24,10.45, 67	-798.70, 10337.00	1.66, 1.22, 67	549.30	1.58	M4Ve	11.28	9.54	25.85
701	18 05 07.58	-3 -1 -52.75	10.60,08.53, 90	570.10, -332.50	1.22, 1.00, 90	128.20	1.44	M1	10.89	9.37	27.13
1224	18 07 32.85	-15 -57 -47.10	...	-617.00, -342.00	5.00, 5.00, 176	132.60	0.00	M4.5	15.44	13.64	27.93
4053	18 18 57.40	66 11 32.40	2000.00,2000.00, 45	464.00, -469.00	100.00, 100.00, 45	137.30	5.30	M4.5	15.29	13.46	27.33
4063	18 34 36.65	40 07 26.44	...	57.00, -203.00	2.00, 2.00, 90	138.00	40.00	M3.5	12.84	11.42	26.92
1230A	18 41 09.86	24 47 13.90	2000.00,2000.00, 2	517.00, 55.00	100.00, 100.00, 45	M4.5	14.00	12.40	27.94
1230B	18 41 09.86	24 47 13.90	2000.00,2000.00, 2	517.00, 53.00	100.00, 100.00, 45	M5	16.10	14.40	27.94

Table 1—Continued

GJ	RA (J2000)	Dec (J2000)	Pos. Err (mas,mas,deg)	PM $_{\alpha}$,PM $_{\delta}$ (mas/yr)	PM $_{err}$ (mas/yr,mas/yr,deg)	Π (mas)	Π_{err} (mas)	Sp	m $_B$	m $_V$	Log L $_X$ (erg s $^{-1}$)
725A	18 42 46.69	59 37 49.42	32.44,27.69, 168	-1327.00, 1801.90	3.61, 3.06, 164	280.20	2.57	M3V	10.45	8.91	26.65
725B	18 42 46.90	59 37 36.65	110.99,102.93, 162	-1393.00, 1845.50	12.19, 11.32, 153	284.40	5.01	M3.5	11.28	9.69	26.65
729	18 49 49.36	-23 -50 -10.44	19.73,12.25, 94	637.57, -192.40	2.23, 1.44, 94	336.40	1.82	M3.5	12.55	10.95	27.78
747A	19 07 43.00	32 32 41.30	...	1235.00, 1130.00	5.00, 5.00, 125	123.00	4.00	M3	13.30	11.70	27.08
747B	19 07 45.00	32 32 54.00	18043.00,18043.00, 138	1213.00, 1095.00	25.00, 25.00, 48	M5	...	12.10	27.08
752A	19 16 55.26	05 10 08.05	11.77,07.86, 87	-578.80, -1331.00	1.33, 0.91, 89	170.20	1.37	M2.5	10.63	9.13	26.94
752B	19 16 57.66	05 09 00.40	2000.00,2000.00, 179	-592.00, -1400.00	100.00, 100.00, 45	170.20	0.00	M8V	19.42	17.30	27.05
1245A	19 53 54.48	44 24 53.30	...	443.00, -581.00	20.00, 20.00, 112	215.00	3.00	M5.5	15.31	13.41	27.47
1245C	19 53 54.90	44 24 54.00	3000.00,3000.00, 45	220.20	0.00	M5.5	...	17.50	27.47
1245B	19 53 55.14	44 24 54.10	...	443.00, -581.00	20.00, 20.00, 112	206.00	3.00	M5.5	15.97	13.99	27.47
791.2	20 29 48.41	09 41 19.30	2000.00,2000.00, 0	704.00, 92.00	100.00, 100.00, 94	112.00	3.00	M4.5V	14.69	13.04	27.89
793	20 30 32.05	65 26 58.42	09.95,07.43, 29	443.24, 284.03	1.15, 0.87, 29	125.60	1.11	M2.5	12.00	10.44	27.77
803	20 45 09.53	-31 -20 -27.24	14.87,06.92, 65	280.37, -360.00	1.68, 0.79, 65	100.50	1.35	M1Ve	10.05	8.61	...
809	20 53 19.79	62 09 15.81	07.04,05.18, 30	1.08, -774.20	0.80, 0.62, 28	141.90	0.77	M0.5	10.03	8.54	27.47
829	21 29 36.81	17 38 35.85	24.71,09.75, 86	1008.00, 376.20	2.91, 1.12, 85	148.20	1.85	M3.5	11.96	10.35	27.47
831A	21 31 17.80	-9 -47 -25.00	M4.5	...	12.60	27.45
4247	22 01 13.12	28 18 24.86	...	372.11, 36.48	3.51, 2.59, 23	111.50	3.19	M4	13.90	11.99	28.36
849	22 09 40.35	-4 -38 -26.62	24.38,11.58, 93	1134.90, -19.71	2.75, 1.30, 91	113.90	2.10	M3.5	11.94	10.42	...
4274	22 23 06.99	-17 -36 -26.40	...	248.00, -895.00	231.00, 64.00, 180	134.10	5.60	M4.5	15.09	13.25	27.80
860A	22 27 59.47	57 41 45.15	27.09,25.47, 64	-870.30, -471.20	3.06, 2.91, 48	249.50	3.03	M3	11.24	9.59	27.72
860B	22 28 00.34	57 41 44.40	2000.00,2000.00, 85	-711.00, -320.00	100.00, 100.00, 80	249.50	0.00	M4	12.90	10.30	27.72
866	22 38 33.62	-15 -17 -59.20	...	2314.00, 2295.00	5.00, 5.00, 13	300.00	5.00	M5.5	14.14	12.18	27.23
867B	22 38 45.31	-20 -36 -52.10	...	427.00, -61.00	7.00, 7.00, 68	M3.5	13.04	11.43	29.31
867A	22 38 45.58	-20 -37 -16.08	108000.00,108000.00, 255	450.59, -79.86	...	115.70	1.50	M1.5	10.57	9.07	29.31
873	22 46 49.73	44 20 02.37	11.83,09.48, 149	-704.60, -459.40	1.40, 1.10, 148	198.00	2.05	M3.5e	11.45	10.09	28.99
876A	22 53 16.73	-14 -15 -49.32	32.97,13.91, 95	960.31, -675.60	3.77, 1.58, 97	212.60	2.10	M4	11.77	10.17	26.49
880	22 56 34.81	16 33 12.36	13.63,07.01, 31	-1033.00, -283.30	1.60, 0.80, 30	145.20	1.22	M1.5V	10.17	8.66	27.09
896A	23 31 52.18	19 56 14.13	19.96,11.30, 60	554.40, -62.61	2.25, 1.28, 56	160.00	2.81	M3.5	11.51	10.32	29.06
896B	23 31 52.56	19 56 13.90	...	602.00, 17.00	14.00, 9.00, 0	160.00	0.00	M4.5	14.40	12.40	29.06
905	23 41 55.01	44 10 38.90	...	100.00, -1594.00	5.00, 5.00, 173	315.00	2.00	M5.5V	14.19	12.28	27.10
1289	23 43 06.28	36 32 14.00	2000.00,2000.00, 45	930.00, -136.00	100.00, 100.00, 0	M4	14.27	12.67	27.69
4360	23 45 31.27	-16 -10 -19.30	2000.00,2000.00, 177	-395.00, -558.00	M5	14.80	14.50	27.66
908	23 49 12.53	02 24 04.40	19.28,06.30, 81	995.31, -968.40	2.33, 0.77, 82	167.50	1.49	M1	10.46	8.98	27.12

Table 2. Detected Stars

GJ	Epoch (YYYYMMDD)	Flux Density (μJy)
53B	20050825	350 ± 86
65B	20050807	4271 ± 66
84	20050807	196 ± 57
102	20050807	182 ± 49
...	20050825	< 204
109	20050612	131 ± 40
...	20050709	< 138
412B	20050612	152 ± 45
...	20050711	< 189
...	20050903	1300 ± 66
557	20050612	236 ± 68
644C	20050816	< 171
...	20050824	224 ± 57
661AB	20050816	536 ± 52
...	20050822	< 147
686	20050609	122 ± 39
...	20050711	< 147
729	20050816	261 ± 59
...	20050822	220 ± 52
747A	20050809	450 ± 133
...	20050824	< 255
803	20050609	1232 ± 50
...	20050612	368 ± 53
...	20050711	222 ± 59
...	20050729	324 ± 49
866	20050709	158 ± 46
867B	20050824	376 ± 64
873	20050824	546 ± 90
896A	20050807	567 ± 52
...	20050825	1027 ± 62

Table 2—Continued

GJ	Epoch (YYYYMMDD)	Flux Density (μJy)
1005A	20050807	< 204
...	20050825	348 ± 96
1116AB	20050903	1482 ± 82
1207	20050816	780 ± 63
...	20050824	195 ± 58
1224	20050816	1271 ± 69
...	20050824	185 ± 59
1230AB	20050809	< 171
...	20050824	199 ± 61
2066	20050709	364 ± 55
...	20050711	< 177
3146	20050809	< 267
...	20050825	281 ± 71
3789	20050816	6203 ± 105
...	20050824	3139 ± 65
4063	20050822	< 150
...	20050816	219 ± 53
4247	20050816	3054 ± 75
...	20050822	791 ± 66
4360	20050807	2174 ± 130
...	20050825	< 300

Table 3. Undetected Stars

GJ	Epoch (YYYYMMDD)	Flux Density Limit (μJy)
15AB	20050612	< 123
...	20050709	< 144
48	20050612	< 132
...	20050709	< 147
54.1	20050807	< 567
83.1	20050809	< 243
...	20050825	< 210
105C	20050807	< 201
...	20050825	< 231
144.0	20050709	< 144
...	20050711	< 105
166C	20050807	< 618
169.1A	20050809	< 234
...	20050825	< 231
176	20050709	< 216
...	20050711	< 255
205	20050709	< 153
...	20050711	< 144
226	20050612	< 141
...	20050709	< 156
251	20050722	< 180
273	20050709	< 156
...	20050711	< 162
338A	20050709	< 156
...	20050711	< 120
382	20050722	< 147
388	20050903	< 567
393	20050722	< 156
406	20050903	< 735
408	20050612	< 126

Table 3—Continued

GJ	Epoch (YYYYMMDD)	Flux Density Limit (μJy)
...	20050722	< 141
411	20050612	< 138
...	20050722	< 186
...	20050903	< 192
412A	20050612	< 141
...	20050711	< 189
...	20050903	< 198
424	20050612	< 225
...	20050709	< 180
...	20050711	< 192
...	20050903	< 204
436	20050612	< 138
...	20050722	< 156
445	20050612	< 171
...	20050903	< 225
450	20050612	< 132
...	20050903	< 189
451B	20050816	< 393
...	20050824	< 243
473AB	20050824	< 180
486	20050612	< 129
493.1	20050824	< 183
504	20050612	< 159
...	20050722	< 144
514	20050612	< 117
...	20050722	< 132
526	20050612	< 177
...	20050722	< 153
566A	20050609	< 141
...	20050722	< 144

Table 3—Continued

GJ	Epoch (YYYYMMDD)	Flux Density Limit (μJy)
569AB	20050609	< 147
570B	20050824	< 285
...	20050824	< 285
581	20050612	< 117
625	20050612	< 129
...	20050711	< 153
628	20050816	< 252
...	20050824	< 192
638	20050612	< 120
...	20050711	< 153
643	20050816	< 189
...	20050824	< 171
644AB	20050816	< 171
...	20050824	< 171
673	20050609	< 111
...	20050711	< 156
687	20050612	< 126
...	20050709	< 162
694	20050612	< 129
...	20050711	< 150
695BC	20050816	< 270
...	20050822	< 240
699	20050609	< 123
...	20050711	< 153
701	20050609	< 123
...	20050711	< 171
725A	20050612	< 141
...	20050709	< 168
725B	20050612	< 141
...	20050709	< 168

Table 3—Continued

GJ	Epoch (YYYYMMDD)	Flux Density Limit (μ Jy)
747B	20050809	< 441
...	20050824	< 255
752AB	20050609	< 144
...	20050711	< 171
791.2	20050822	< 210
793	20050612	< 123
...	20050709	< 159
809	20050612	< 153
...	20050709	< 189
829	20050609	< 144
...	20050711	< 267
831A	20050825	< 231
849	20050609	< 27
...	20050612	< 273
860AB	20050612	< 216
...	20050709	< 225
867A	20050824	< 192
876A	20050609	< 219
...	20050612	< 201
...	20050709	< 186
880	20050609	< 129
...	20050612	< 114
...	20050709	< 162
896B	20050807	< 162
...	20050825	< 186
905	20050824	< 174
908	20050612	< 105
...	20050709	< 123
1156	20050824	< 243
1245ABC	20050809	< 219

Table 3—Continued

GJ	Epoch (YYYYMMDD)	Flux Density Limit (μ Jy)
...	20050825	< 192
1289	20050824	< 459
2005BC	20050807	< 1254
...	20050825	< 420
3076	20050807	< 537
...	20050825	< 264
3125	20050816	< 414
3193B	20050809	< 198
3304	20050809	< 339
...	20050824	< 249
3820	20050824	< 207
4053	20050816	< 159
...	20050822	< 150
4274	20050824	< 198

Table 4. VLBA Observations of M dwarfs

GJ	Date	Beam Sizes (mas, mas)	Beam PA (deg)	Image RMS μ Jy
65B	23 MAR 2006 A	(3.5, 1.5)	-10.7	163
65B	23 MAR 2006 B	(4.2, 1.8)	11.4	141
65B	25 MAR 2006 A	(3.4, 1.4)	-15.7	157
65B	25 MAR 2006 B	(2.8, 2.0)	8.4	118
65B	26 MAR 2006 A	(3.5, 1.5)	-13.6	147
65B	26 MAR 2006 B	(2.7, 2.1)	9.1	121
285	21 MAR 2006	(2.1, 0.9)	-1.1	90
285	24 MAR 2006	(2.5, 1.0)	13.4	109
285	27 MAR 2006	(2.7, 1.1)	15.9	111
412B	25 MAR 2006	(2.4, 0.9)	-11.2	109
412B	30 MAR 2006	(2.2, 1.2)	-12.7	86
412B	01 APR 2006	(2.2, 0.9)	-12.8	86
803	10 MAY 2006	(3.2, 1.9)	5.3	111
803	20 MAY 2006	(3.2, 1.6)	6.0	111
803	21 MAY 2006	(3.3, 1.7)	8.2	109
896A	23 MAR 2006	(2.6, 1.5)	2.3	89
896A	25 MAR 2006	(2.4, 1.0)	-10.9	85
896A	26 MAR 2006	(2.4, 1.0)	-10.2	88
1224	10 MAY 2006	(2.9, 2.0)	12.3	88
1224	20 MAY 2006	(3.0, 1.6)	-0.5	104
1224	21 MAY 2006	(2.9, 1.8)	0.6	102
4247	23 MAR 2006	(2.4, 1.6)	-5.2	95
4247	25 MAR 2006	(2.1, 1.1)	-16.6	85
4247	26 MAR 2006	(2.2, 1.1)	-16.2	87

Table 5. Positions of Astrometric Calibrators

GJ	Calibrator	Flux (mJy)	α	δ	Type
65B	J0132-1654	1294.0 ± 5.7	01 32 43.487468	-16 54 48.522043	primary
...	J0142-1633	38.4 ± 1.2	01 42 45.261198 \pm 00.000014	-16 33 07.196786 \pm 00.000121	secondary
285	J0739+0137	463.6 ± 2.2	07 39 18.033892	01 37 04.617926	primary
...	J0751+0152	50.4 ± 1.4	07 51 02.281590 \pm 00.000002	01 52 15.761011 \pm 00.000023	secondary
412B	J1108+4330	368.6 ± 1.6	11 08 23.476932	43 30 53.657076	primary
...	J1110+4403	103.7 ± 2.6	11 10 46.345812 \pm 00.000003	44 03 25.925528 \pm 00.000028	secondary
803	J2056-3208	594.5 ± 4.4	20 56 25.070234	-32 08 47.800507	primary
...	J2042-3152	62.6 ± 0.6	20 42 46.406548 \pm 00.000075	-31 52 28.592351 \pm 00.002223	secondary
896A	J2328+1929	119.4 ± 0.8	23 28 24.874755	19 29 58.030041	primary
...	J2334+2010	62.2 ± 1.9	23 34 14.156496 \pm 00.000009	20 10 28.882640 \pm 00.000279	secondary
1224	J1753-1843	110.4 ± 0.5	17 53 09.088754	-18 43 38.523184	primary
...	J1825-1718	69.1 ± 0.3	18 25 36.532398 \pm 00.000029	-17 18 49.849551 \pm 00.002606	secondary
...	J1809-1520	16.4 ± 0.2	18 09 10.208891 \pm 00.001145	-15 20 09.692410 \pm 00.030386	secondary
4247	J2205+2926	141.5 ± 0.6	22 05 46.506426	29 26 55.131163	primary
...	J2203+2811	56.8 ± 1.5	22 03 59.147970 \pm 00.000004	28 11 21.869208 \pm 00.000015	secondary

Table 6. Positions of Stars

GJ	MJD	Flux (mJy)	RA (J2000)	Dec. (J2000)	$\Delta\alpha$ (mas)	$\Delta\delta$ (mas)	$\Delta\alpha_{\text{opt}}$ (mas)	$\Delta\delta_{\text{opt}}$ (mas)
65B	53817.78	2.171 ± 0.482	$01\ 39\ 02.990153 \pm 0.000014$	$-17\ 56\ 57.918175 \pm 00.000342$	0.000 ± 0.198	0.000 ± 0.342	319.940 ± 155.000	264.745 ± 155.000
...	53817.89	1.800 ± 0.340	$01\ 39\ 02.990308 \pm 0.000011$	$-17\ 56\ 57.918094 \pm 00.000287$	2.208 ± 0.161	0.081 ± 0.287	320.487 ± 155.000	264.289 ± 155.000
...	53819.89	1.872 ± 0.289	$01\ 39\ 02.992267 \pm 0.000008$	$-17\ 56\ 57.906928 \pm 00.000202$	30.158 ± 0.116	11.247 ± 0.202	319.378 ± 155.000	266.167 ± 155.000
...	53820.89	2.075 ± 0.443	$01\ 39\ 02.993345 \pm 0.000016$	$-17\ 56\ 57.902321 \pm 00.000456$	45.551 ± 0.229	15.854 ± 0.456	320.182 ± 155.000	266.183 ± 155.001
285	53815.14	1.476 ± 0.275	$07\ 44\ 40.017980 \pm 0.000006$	$03\ 33\ 6.109089 \pm 00.000163$	0.000 ± 0.088	0.000 ± 0.163	-45.984 ± 41.247	73.853 ± 35.409
...	53818.14	0.553 ± 0.100	$07\ 44\ 40.017550 \pm 0.000007$	$03\ 33\ 6.108662 \pm 00.000208$	-6.436 ± 0.112	-0.427 ± 0.208	-46.170 ± 41.247	74.115 ± 35.409
803	53865.20	1.772 ± 0.310	$20\ 45\ 09.679701 \pm 0.000011$	$-31\ 20\ 29.507331 \pm 00.000290$	0.000 ± 0.135	0.000 ± 0.290	17.516 ± 26.115	-3.153 ± 19.137
896A	53817.81	0.929 ± 0.203	$23\ 31\ 52.433685 \pm 0.000008$	$19\ 56\ 13.712351 \pm 00.000171$	0.000 ± 0.112	0.000 ± 0.171	114.239 ± 35.428	20.565 ± 28.187
...	53819.81	1.399 ± 0.298	$23\ 31\ 52.434263 \pm 0.000013$	$19\ 56\ 13.714736 \pm 00.000202$	8.148 ± 0.183	2.385 ± 0.202	114.366 ± 35.428	20.924 ± 28.187
...	53820.81	3.895 ± 0.230	$23\ 31\ 52.434540 \pm 0.000002$	$19\ 56\ 13.715419 \pm 00.000045$	12.059 ± 0.031	3.068 ± 0.045	114.281 ± 35.428	20.572 ± 28.186
4247	53817.79	0.950 ± 0.201	$22\ 01\ 13.304385 \pm 0.000008$	$28\ 18\ 25.130036 \pm 00.000173$	0.000 ± 0.104	0.000 ± 0.173	7.147 ± 122.891	85.510 ± 90.706
...	53819.79	1.161 ± 0.300	$22\ 01\ 13.304782 \pm 0.000016$	$28\ 18\ 25.132249 \pm 00.000257$	5.247 ± 0.207	2.213 ± 0.257	7.392 ± 122.892	85.268 ± 90.706
...	53820.79	1.164 ± 0.257	$22\ 01\ 13.304933 \pm 0.000011$	$28\ 18\ 25.134030 \pm 00.000196$	7.242 ± 0.148	3.994 ± 0.196	6.914 ± 122.891	85.804 ± 90.706

Table 7. Proper Motion and Acceleration Relative to Optical Astrometry

GJ	$\Delta\mu_\alpha$ (mas y ⁻¹)	$\Delta\mu_\delta$ (mas y ⁻¹)	a_α (AU y ⁻²)	a_δ (AU y ⁻²)
65B	37.3 ± 52.5	-218.5 ± 38.8	0.0032 ± 0.0045	-0.0189 ± 0.0033
285	22.4 ± 12.5	-32.1 ± 22.7	0.0088 ± 0.0049	-0.0127 ± 0.0090
896A	-7.4 ± 7.2	-10.1 ± 24.5	-0.0031 ± 0.0030	-0.0042 ± 0.0102
4247	18.1 ± 27.8	-24.4 ± 30.3	0.0046 ± 0.0071	-0.0062 ± 0.0078

Table 8. Limits in Companion Mass and Semi-Major Axis

GJ	r_{min} (AU)	$M_{p,min}$ (M_J)	$M_{p,0.3}$ (M_J)	$M_{p,3}$ (M_J)
65B	1.3	4.5	19	24
285	0.8	3.3	9	42
896A	0.8	3.8	10	42
4247	1.0	6.1	21	44